Received: 17 February 2023 | Revised: 21 April 2023 | Accepted: 25 April 2023

DOI: 10.1002/jlcr.4029

Journal of Labelled Compounds and Radiopharmaceuticals WILEY

REVIEW

The inverse electron demand Diels–Alder cycloaddition with carbon-11 and fluorine-18: A gateway to pretargeted imaging across the blood–brain barrier

Simon H. Zientek | Stephen Thompson | Selena Milicevic Sephton | Franklin I. Aigbirhio

Department of Clinical Neurosciences, University of Cambridge, Cambridge, UK

Correspondence
Stephen Thompson, Department of Clinical Neurosciences, University of Cambridge, Cambridge CB2 0SZ, UK.
Email: st534@cam.ac.uk

There is increased focus on developing tools to image large biomolecules, such as antibodies, within the brain using positron emission tomography (PET). The inverse electron demand Diels–Alder cycloaddition (IEDDA) reaction has offered the greatest prospect of achieving such a feat and has gained much interest over the past decade. The fast reaction kinetics of the IEDDA reaction opens up the possibility of utilising a pretargeted approach, whereby the subject is pretreated with a biomolecule that has high specificity for its target. A radiolabelled second component is then administered to the subject, enabling the biomolecule to be visualised by PET. However, for this to become common practice, there is a need for the development of either radiolabelled *trans*-cyclooctenes (TCOs) or tetrazines that can cross the blood–brain barrier (BBB). This review highlights the advancements in the development of both radiolabelled TCOs and tetrazines, which have been radiolabelled with either carbon-11 or fluorine-18 and show promise or have been evaluated for use in pretargeted PET imaging across the BBB.

KEYWORDS

blood–brain barrier, carbon-11, inverse electron demand Diels-Alder reaction, pretargeted imaging, tetrazine, trans-cyclooctene

1 | INTRODUCTION

Positron emission tomography (PET) is a molecular imaging technique that enables visualisation and quantification of targets of interest by application of radiolabelled molecules, which bear positron-emitting radionuclides.[1] For application in brain imaging, a radiolabelled molecule must cross the blood–brain barrier (BBB). This therefore represents the largest challenge in the development of a novel or improved PET radiotracer for neuroimaging.

Pretargeted imaging (Figure 1) has emerged as a powerful strategy to enable rapid imaging with PET radiotracers that would usually be slow to distribute to and accumulate at their target of interest within the body.[2] To achieve this, pretargeted imaging (Figure 1) makes use of a first component that bears a targeting molecule (e.g., antibody or high affinity antibody fragments) as

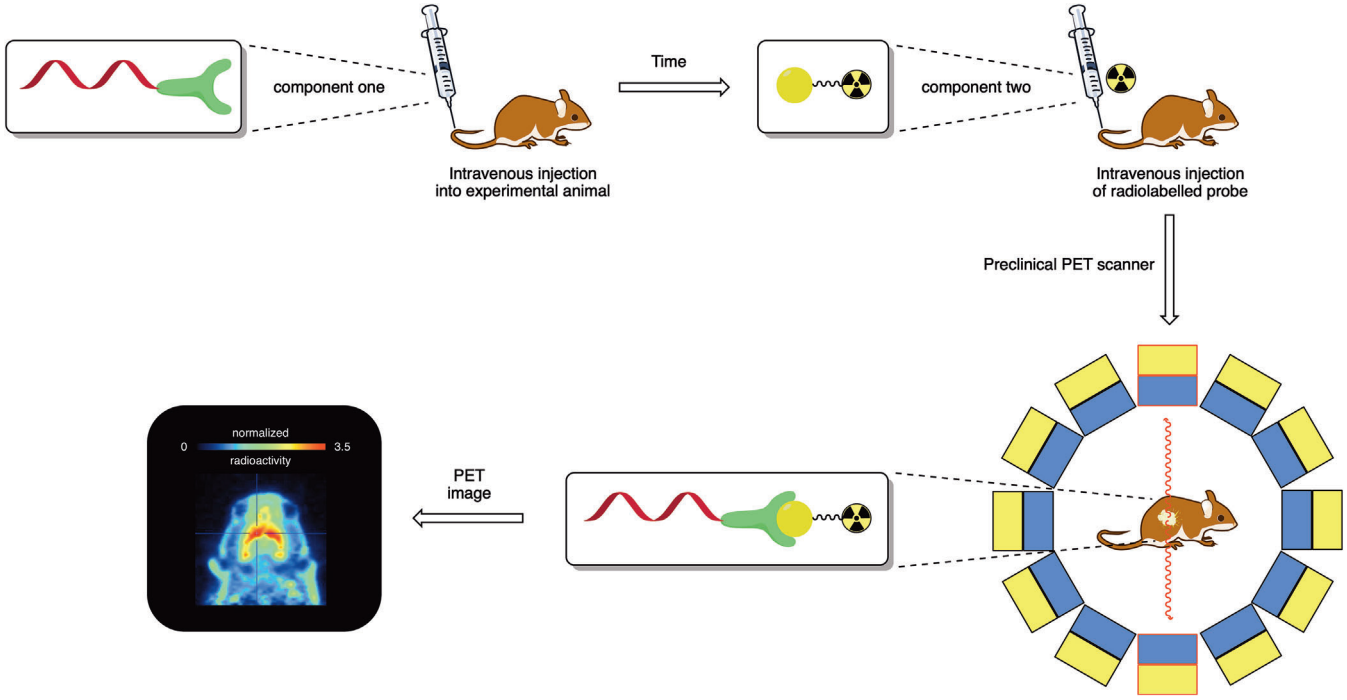

FIGURE 1 The concept of pretargeted imaging. The first component is pre-administered to a subject and allowed to distribute in the body for a predetermined time. At this point, the second radiolabelled component is administered, and the PET imaging experiment is started.

well as a reactive handle and a second component that bears a radioactive label and a second complimentary reactive handle. The first component is administered to the test subject and allowed to slowly distribute through the body and tissues for a pre-determined amount of time—usually hours or days before the PET scan. After this pre-distribution period, the second radiolabelled component is administered and rapidly distributes around the body. When it encounters the first component, the two complementary species rapidly ligate. A short period of time is passed to allow any of the unreacted second component to clear from the body, before a PET scan is conducted to visualise the distribution of the target molecule within the body.

Whilst pretargeted imaging with antibodies or high affinity antibody fragments has primarily seen application within oncology, the same strategy could be applied to PET imaging in the brain. The main limitation in the application of pretargeting in the brain remains getting both the targeting molecule (e.g., antibody or high affinity antibody fragment) and radiolabelled small molecule across the BBB. The pretargeted strategy can be tailored to account for poorly or non-permeable molecules, for example, by incorporating the radiolabel on the small brain-permeable component and using a delivery vector to shuttle the targeting molecule across the BBB. This review focuses on the radiosynthesis and characterisation of the radiolabelled small molecule components of the

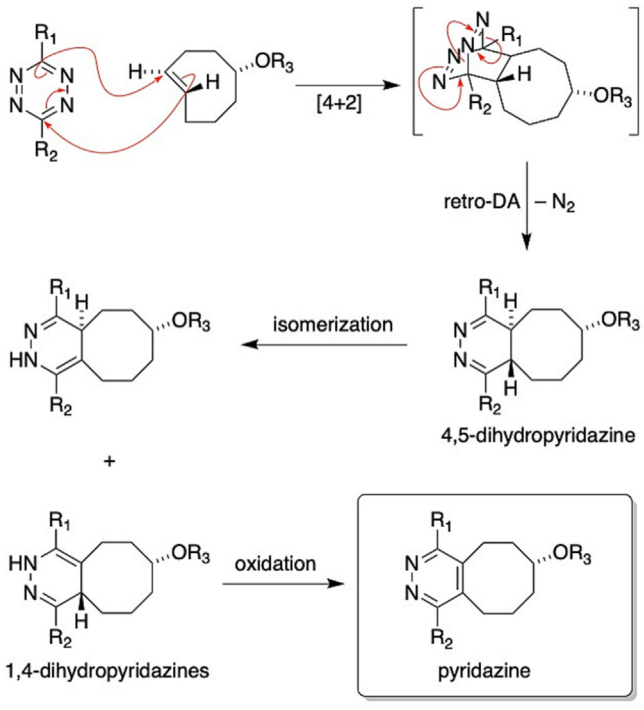

SCHEME 1 The mechanism of the IEDDA reaction between a tetrazine diene and *trans*-cyclooctene dienophile.

pretargeted approach, and readers are directed to the literature for discussion of strategies for the delivery of targeting molecules across the BBB.[3–9]

In chemistry terms, pretargeted imaging makes use of bioorthogonal reactions, which are defined as 'chemical reactions that neither interact nor interfere with a biological system'.[10,11] Although biorthogonal reactions share some features with bioconjugation reactions such as fast rate constants and occur at physiological pH, in physiological media in a chemoselective manner, they do not interfere with the biological system under study. Although many different types of chemical transformations can be defined as bioorthogonal, pretargeted PET imaging has almost exclusively been focused around the application of the inverse electron demand Diels–Alder cycloaddition (IEDDA) reaction. The IEDDA cycloaddition between a tetrazine and a *trans*-cyclooctene (TCO, Scheme 1) is arguably the ideal biorthogonal reaction—it is catalyst-free and has fast kinetics under physiological conditions. The IEDDA reaction is a type of cyclization reaction whereby the electronic demand is reversed between the reacting partners, the diene and the dienophile.[12] In contrast to the classical DA reaction, in the IEDDA reaction, an electron poor diene (in this case, a tetrazine) reacts with an electron rich dienophile (in this case, a TCO, Scheme 1) to yield a cyclized product without a need for a catalyst (e.g., copper). This reactivity is the product of a smaller electronic gap between the HOMO of the dienophile and LUMO of the diene.[13] It has been shown that electron-donating groups raise the HOMO of the dienophile and electron-withdrawing groups lower the LUMO of the diene. Although the mechanism of the IEDDA reaction is still debated, the most accepted pathway involves a [4 + 2] cycloaddition of a tetrazine diene with the alkene, followed by a retro-Diels–Alder reaction promoted by departure of gaseous nitrogen to relieve the ring strain in the bicyclic ring, which in turn affords a 4,5-dihydropyridazine.[12] Then, the 4,5-dihydropyridazine undergoes either isomerization to yield a 1,4-dihydropyridazine or oxidation to give a fully aromatized pyridazine.

Extensive investigation of the kinetic factors and reaction mechanism of the IEDDA reaction has been performed by several research groups, which has been reviewed elsewhere, and the reader is directed towards this extensive literature.[12] Owing to the properties described above, the IEDDA reaction has been an attractive chemical transformation to achieve pretargeted PET imaging. For this purpose, the most widely exploited IEDDA reaction is that between specifically functionalized TCOs and tetrazines (Scheme 1) as reaction components. Studies have determined rates of reaction between many different tetrazines and TCOs (see Figures 2 and 3), providing a guide to selecting the most appropriate reaction components.[12] These studies have demonstrated that lowering the LUMO energy of the tetrazines, usually achieved by the incorporation of increasingly electron-withdrawing substituents, increases the rate of reaction (Figure 2). The increase in reactivity of the tetrazines is, however, coupled with a decrease in their chemical stability in biological reaction media as the resultant tetrazines are more susceptible to nucleophilic attack. Recently, Svatunek et al.[15] showed that the increase in reactivity by incorporation of 2-pyridyl substituents is a result of distortion of tetrazine ring due to N-N repulsion, rather than by the electronic properties of the substituent. The authors also showed that vinyl ether substituted tetrazines maintained similar reactivity to 2-pyridyl tetrazines due to N-O repulsion and distortion of the tetrazine but were much less prone to nucleophilic attack and resultingly were significantly more stable in biological

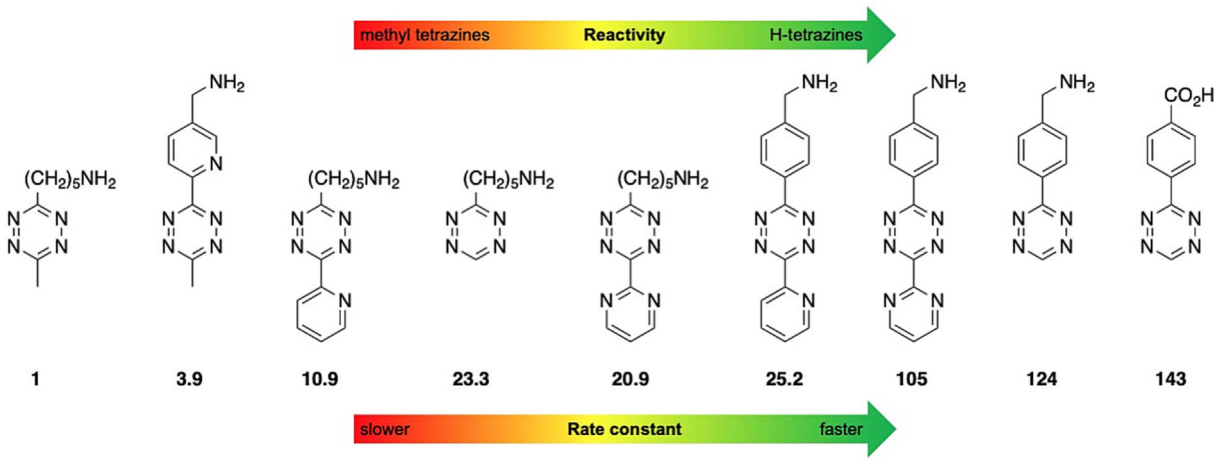

FIGURE 2 Reactivity of selected tetrazine dienophiles, adapted from Oliveira et al.,[13] showing rate constants relative to reactivity for both di-substituted (s-tetrazines) and mono-substituted (h-tetrazines) tetrazines. Relative ratios of the rate constants standardised to aminopentyl-methyl tetrazine (far left) are shown under each structure.[14]

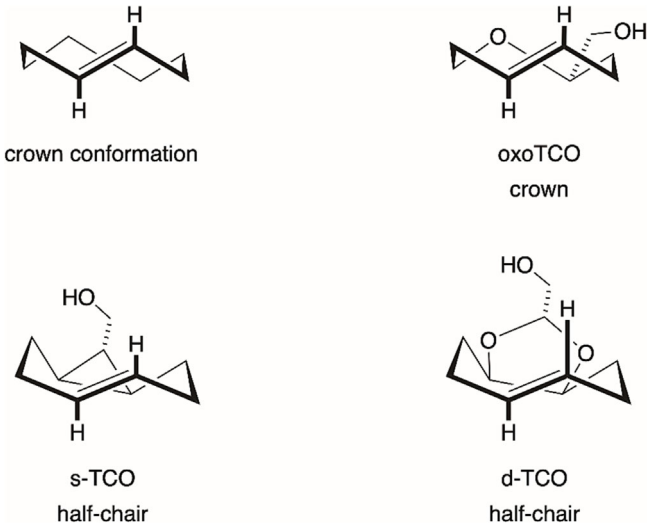

FIGURE 3 Nomenclature and reactivity of TCOs: s-TCO and d-TCO adopt half-chair conformation making them more reactive, whereas higher reactivity of oxoTCO, which adopts crown conformation, is likely due to electron density of oxygen in the ring.

media. Whilst the vinyl-ether type tetrazines have yet to be used in the context of PET imaging, they offer a potential solution to challenges in preparing radiolabelled, highly reactive tetrazines.

TCOs can be made more reactive by being 'locked' into a more strained conformation by incorporation of *cis*-fused cyclopropyl or dioxolane rings, or by incorporation of oxygen into the TCO ring, which increases angle strain on the alkene (Figure 3).[16–18] However, there still remains uncertainty whether selected reaction components will yield the desired rapid biorthogonal transformation in vivo.

When designing a pretargeted experiment, it is important to consider which reactive handle is attached to the targeting component and which receives the radiolabel. Arguably, since the targeting component will have a longer residence time in vivo, it would be appended to the more biologically stable reactive handle. For pretargeting using the IDEAA reaction, this means linking the TCO to the pretargeting agent, whilst the tetrazine carries the radiolabel. There are many examples of radiolabelled tetrazines, which have been extensively reviewed by García-Vázquez et al.[19]; however, this review focuses on tetrazines that have potential application within pretargeted PET imaging in the brain.

Tetrazines are less stable in vivo, as they are unstable towards biological nucleophiles such as thiols of cysteine residues or amines of lysine residues. This instability tends to be more pronounced for more reactive and less sterically hindered tetrazines.[14,20,21] Whilst free TCOs tend to also be unstable towards both isomerization and metabolism in vivo, attaching a TCO to a biomolecule using a short linker dramatically increases their stability, particularly towards isomerization to the much less reactive *cis*-cyclooctenes (CCO) isomer, which is mediated by Cu-containing enzymes in the blood plasma.[22,23]

There are well-defined physicochemical characteristics that predict the passive diffusion of molecules across the BBB.[24] For radiolabelled molecules, these predictive characteristics necessitate the use of low molecular weight molecules that are uncharged, which tends to favour carbon-11 and fluorine-18 as preferred radioisotopes. However, radiolabelling with these isotopes generally requires harsh conditions (high temperatures and strong bases) to achieve radiolabelling of a particular scaffold, which tend to be poorly compatible with TCOs, and especially poor for reactive tetrazines. This has been less of a concern in the cancer imaging field, where the unstable tetrazines can be chelated to radioactive metal isotopes under more mild conditions. The combination of poor stability in radiolabelling conditions and poor in vivo stability of the key reaction components has slowed the development of pre-targeted imaging in the brain. Recently, milder ^{18}F-fluorination methodologies have been developed to enable the radiolabelling of small molecular weight tetrazines with fluorine-18, providing potential new tools towards successful pretargeted imaging in the brain (vide infra).

The pharmacokinetic properties of the radiolabelled tetrazine or TCO are also critically important for a successful pretargeted imaging strategy. An ideal radiolabelled fragment would show high initial brain uptake (high peak SUV or %ID/g), maximising the concentration of the tetrazine or TCO for reaction with its complimentary IEDDA reaction partner. The tetrazine or TCO should also exhibit fast washout from the brain, which would indicate that the tetrazine or TCO has minimal off-target binding. Fast washout of the tetrazine or TCO, coupled with rapid systemic clearance, will also improve image contrast in the pretargeted imaging experiment. Peripheral metabolism of the tetrazine or TCO should also not produce any brain-penetrant metabolites, which would interfere with image interpretation and quantification. Finally, the pharmacokinetic properties of the antibody or antibody fragment in relation to the imaging timepoints are also a key consideration when designing imaging experiments using such species. The PET imaging (and treatment) of a variety of cancers and other disorders in the periphery using highly selective and specific monoclonal antibodies and antibody fragments has revolutionised our understanding of these conditions over the last 10 years.[2,25–30] Studies in this area have highlighted the fact that these large molecules tend to be slow to accumulate at their target site and are also slow to clear

from the circulation. When tagged with short-lived radioisotopes, high background signal and reduced image contrast are often observed in the resulting PET images. Two solutions to this problem are to radiolabel the targeting molecule with a longer-lived radioisotope (e.g., ^{89}Zr) and image the subject several days after the administration of the imaging agent or to use clearing agents to react with and promote the clearance of any unbound imaging agent, therefore reducing background signal.[31] However, high radiation doses to patients due to the use of longer lived isotopes are a distinct drawback to this approach. The use of a pretargeting approach with shorter lived isotopes, coupled to appropriate clearing and masking strategies, negates some of these issues, and analogous strategies could similarly be applied when considering pretargeting experiments in the brain.

This review details the results of studies exploring the radiosynthesis of ^{18}F- and ^{11}C-labelled tetrazines and TCOs, highlighting several features of the reported compounds, including the ease of preparation of both required TCO and tetrazine precursors, their chemical as well as in vivo stability, how easily they could be radiolabelled and importantly how well they cross the BBB.

2 | BRAIN PENETRANT TCOS

One of the first examples of a radiolabelled TCO was reported by Li et al.[32] The group originally intended to directly radiolabel a tetrazine with [^{18}F]fluoride, as seen in Scheme 2. However, due to the high reactivity of tetrazine precursors and their poor stability, the desired radiolabelled tetrazine was obtained with a radiochemical yield (RCY) of approximately 1%, and efforts therefore turned to the development of an ^{18}F-lalelled TCO.

As seen in Scheme 3, (*E*)-cyclooct-4-enol **3** was first alkylated with α-bromoacetic acid before being reduced to give alcohol **4**. Photoisomerization of **4** gave TCO **5** before further reaction with 4-nitrobenzenesulfonyl chloride gave the radiolabelling precursor **6** in 26% yield

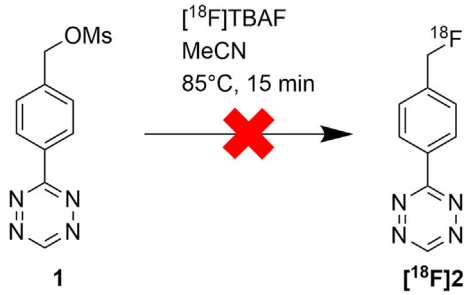

SCHEME 2 The first unsuccessful attempt[32] to directly radiolabel a tetrazine with fluorine-18.

over four steps. A variety of conditions were screened for the radiofluorination of **6** with the highest RCY achieved through reaction of **6** with [^{18}F]fluoride (100 mCi, 3.7 GBq) and tetrabutylammonium bicarbonate in acetonitrile (MeCN) at 75°C for 15 min. This gave [^{18}F]**7** with a decay corrected RCY (d.c RCY) of 71%. [^{18}F]**7** was then reacted with 3,6-di(2-pyridyl)-*s*-tetrazine to investigate its performance in the IEDDA reaction. High performance liquid chromatography (HPLC) determined that the reaction was complete within 10 s, yielding the 1,2-dihydropyrazine product in d.c RCY > 98%. Minimal isomerisation to the 1,4-dihydropyrazine adduct was also observed (1% RCY).[32]

In 2014, Wyffels et al.[22] investigated the brain permeability and pharmacokinetic profile of [^{18}F]**7**. The radiochemical synthesis was modified and automated on a Veenstra FluroSynthon III synthesis module. Starting from a tosylate precursor, [^{18}F]**7** was radiolabelled using [^{18}F]KF•Kryptofix® *222* (K*222*®)•K_2CO_3 in MeCN at 90°C for 10 min. [^{18}F]**7** was synthesised in a total time of 55 min from end of bombardment (EOB) with a d.c. RCY of 14 ± 5% and a radiochemical purity of >99%. The stability of [^{18}F]**7** was assessed by radio-HPLC and was found to be stable for up to 4 h in saline. [^{18}F]**7** had a log*D* of 1.68 ± 0.02 (shake-flask method), which is suitable for BBB permeability.[33,34] The ability of [^{18}F]**7** to cross the BBB was assessed in adult C57BL/6 J mice using microPET scans and post-scan ex vivo biodistribution studies. From the microPET images, [^{18}F]**7** was able to cross the BBB, with high uptake after 1 min p.i., followed by fast washout. However, after 60 min, a steady increase in uptake was observed in the time-activity curve peaking at 120 min, suggestive of the formation of BBB penetrant radiometabolites. Ex vivo biodistribution corroborates with the preclinical PET data with high brain uptake seen at 5 min post injection (p.i.) of 3.74 ± 0.68% ID/g decreasing to 3.03 ± 0.52% ID/g at 30 min p.i., before rising to 3.66 ± 0.84% ID/g at 120 min p.i. At 120 min p.i. skeletal uptake was also observed, which was suggestive of defluorination. Regional uptake of [^{18}F]**7** was investigated with ex vivo autoradiography, which showed a homogeneous distribution across the brain.

Finally, with evidence to suggest that [^{18}F]**7** was unfavourably metabolised in vivo, the formation of radiometabolites was investigated both in vitro and in vivo. In vitro evaluation in human liver microsomes showed poor stability with only 13.2 ± 1.2% of [^{18}F]**7** remaining after 5 min. In vivo evaluation in mouse plasma after 5 min p.i. found an equally poor level of stability by radio-HPLC. Only 10.7 ± 5.6% of the parent molecule was intact and four polar radiometabolites were also observed. Stability was better, albeit still poor in the brain with 32.2 ± 5.8% of the parent molecule remaining 5 min

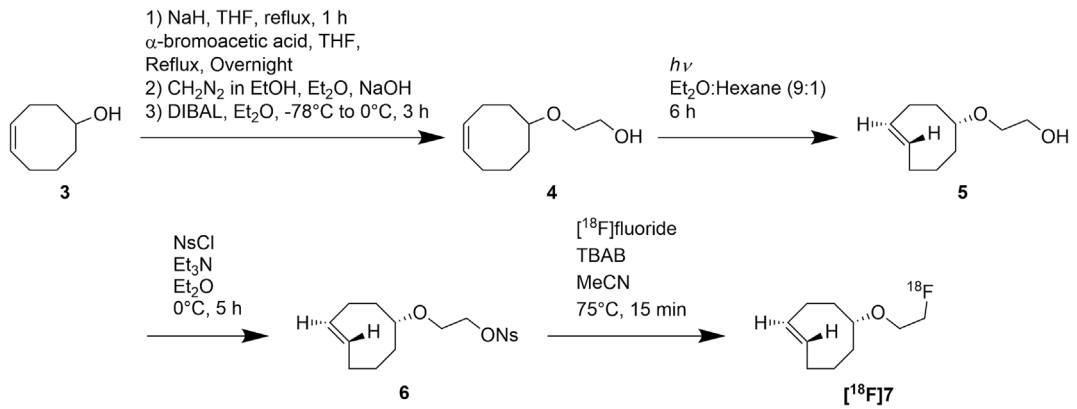

SCHEME 3 Synthesis of radiochemical precursor **6** and radiochemical synthesis of [^{18}F]**7**.

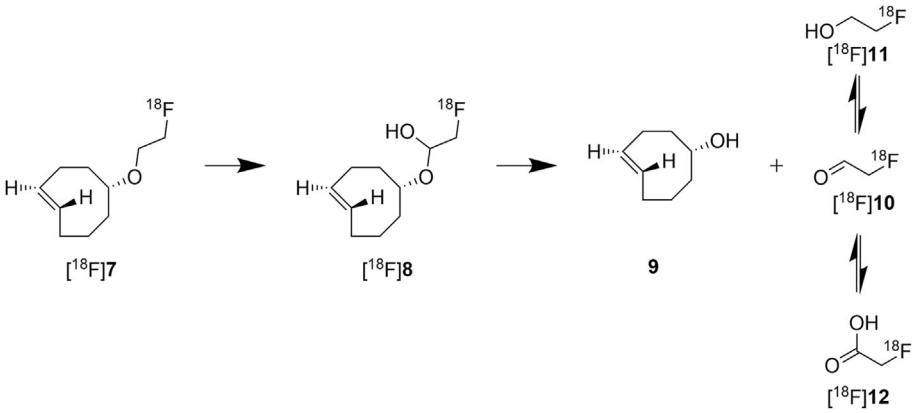

SCHEME 4 The proposed metabolic pathway of [^{18}F]**7** involves the release of [^{18}F]fluoroacetaldehyde, [^{18}F]**10**, which can be converted to either 2-[^{18}F]fluoroethanol, [^{18}F]**11** or 2-[^{18}F]fluoroacetic acid, [^{18}F]**12**.[22]

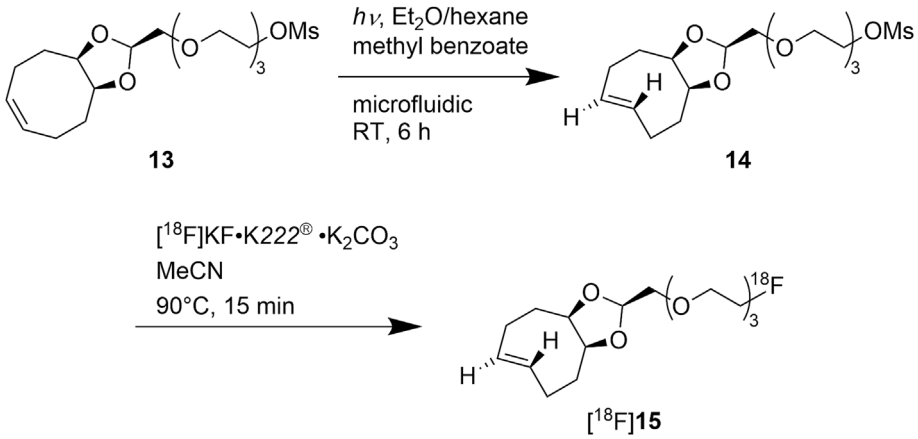

SCHEME 5 Synthesis of radiochemical precursor **14** and radiosynthesis[35] of [^{18}F]**15**.

p.i., along with three other polar radiometabolites. A hypothesis for the metabolic pathway was proposed, as shown in Scheme 4.[22] Ultimately, the inadequate metabolic profile of [^{18}F]**7** precluded its use in pretargeted imaging within the brain.

Efforts have since focused on the development of more reactive TCO frameworks, with several reported to be able to cross the BBB. With the aid of computational modelling, Darko et al.[17] designed and explored the reactivity and stability of conformationally strained dioxolane-fused *trans*-cyclooctenes (d-TCOs) identifying that this framework showed fast reaction kinetics for the IEDDA whilst having increased stability. Building on this, Billaud et al.[35] synthesised [^{18}F]**15** based on the d-TCO framework (Scheme 5). The precursor was prepared from a dioxolane-fused *cis*-cyclooctene (d-CCO) with a triethylene glycol chain, which was modified to bear a mesylate leaving group. Photoisomerization of d-CCO **13** was performed on an in-house microfluidic system, which gave the d-TCO precursor **14** in 44% yield. On an

inhouse built module, **14** was radiolabelled through a semi-automated process using [^{18}F]KF•K*222*®•K_2CO_3 in MeCN at 90°C for 15 min. After HPLC purification and formulation, [^{18}F]**15** was synthesised in a total time of 60 min with a d.c. RCY yield of 12%, radiochemical purity of >99% and molar activity of 70–188 GBq/μmol.[35] Importantly, minimal isomerisation from the *trans* isomer to the *cis* isomer (<1%) was observed during radiosynthesis.

The in vitro stability of [^{18}F]**15** was assessed in phosphate buffered saline (PBS, pH 7.4) and rat plasma. In PBS, [^{18}F]**15** showed good stability with 94% of the parent molecule intact after 2 h of incubation at 37°C. However, in rat plasma, [^{18}F]**15** decreased to 52% after 1 h and 34% after 2 h after incubation at 37°C, with isomerization from the *trans* to *cis* isomer observed. It was, however, unclear if any other radiometabolites were observed. The authors postulated that due to the fast reaction kinetics of the IEDDA, the plasma stability of [^{18}F]**15** would not have a detrimental effect on its in vivo performance.[35] Therefore, [^{18}F]**15** was further evaluated in a biodistribution and a proof of principle pretargeted PET study.

Biodistribution was performed in healthy NMRI mice over the course of 60 min. Defluorination of [^{18}F]**15** was not seen with a standard uptake value (SUV) of 0.3 ± 0.0 observed in bone at 60 min p.i., and [^{18}F]**15** was able to cross the BBB with an SUV of 1.3 ± 0.2 at 2 min p.i. and 0.6 ± 0.0 at 60 min p.i. observed in the brain. At 15 min, only 20.8 ± 1.1% of the parent molecule was isolated in the brain by radio-HPLC, suggesting that [^{18}F]**15** was rapidly metabolised, generating brain penetrant metabolites. In vivo microPET scans were then performed in LNCaP prostate tumour-bearing mice. A tetrazine coupled to a pseudo peptide that had an affinity for prostate-specific membrane antigen (PSMA) was administered to the mice, and after a 10 min period, [^{18}F]**15** was administered. The tumour was visible 2 h p.i., with higher uptake seen in the tumour in the right shoulder compared to muscle in the left shoulder.[35] Billaud et al.[36] have further evaluated [^{18}F]**15** in a pretargeted immuno-PET study in an ovarian carcinoma model, using tetrazine-labelled antibodies for human epidermal growth factor receptor 2 as the pre-targeting agent.

In 2020, Ruivo et al.[37] developed two new radiolabelled d-TCOs, [^{18}F]MICA-212, [^{18}F]**16** and [^{18}F]MICA-213, [^{18}F]**17**, as seen in Figure 4. [^{18}F]**16** was radiolabelled from a tosylate precursor using [^{18}F]KF•K*222*®•K_2CO_3 in MeCN at 100°C for 5 min giving the desired product in 8.7 ± 0.4% d.c. RCY (from end of bombardment [EOB]) and radiochemical purity of 98%. [^{18}F]**17** was radiolabelled from a 2-chloropyridinyl precursor through a halogen exchange reaction. The precursor was radiolabelled with [^{18}F]KF•K*222*®•K_2CO_3 in DMF at 130°C for 5 min giving [^{18}F]**17** a d.c. RCY from EOB of 5.5 ± 0.5% and radiochemical purity of 98%. Lipophilicity of both molecules was assessed via the shake flask method, and the log*D* was determined to be 1.30 ± 0.03 for [^{18}F]**16** and 1.73 ± 0.01 for [^{18}F]**17**, which was promising for passive BBB passage.[33,34] The in vitro stability of both probes was then investigated in both PBS and mouse plasma after incubation for 2 h at 37°C. Both radioligands show excellent stability in PBS, whereas in

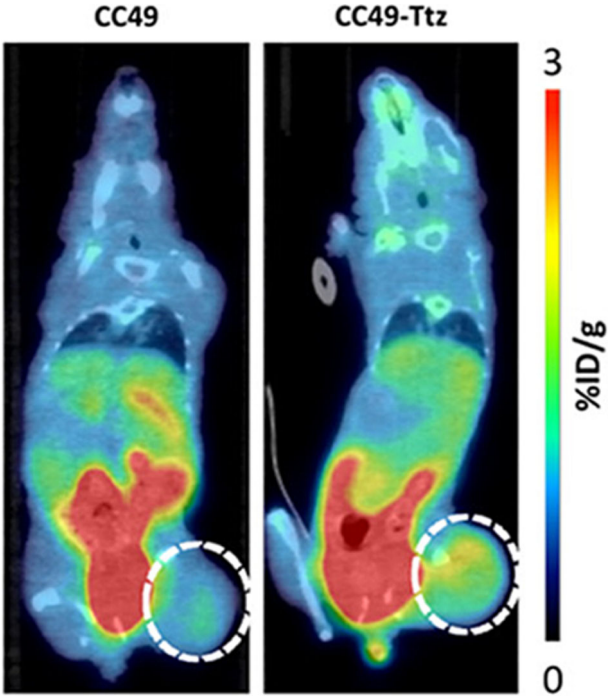

FIGURE 5 Static image at 60 min p.i. of [^{18}F]**17** in LS174T tumour-bearing mice pre-treated (24 h prior) with either an unmodified CC49 antibody (left) or a tetrazine-tagged CC49 antibody (right). Increased tumour visualisation was seen with mice pre-treated with a tetrazine tag CC49 antibody (right). Reproduced from https://doi.org/10.1021/acsomega.9b03584 with permission from the American Chemistry Society. Further permission related to this figure should be directed to the ACS.[37]

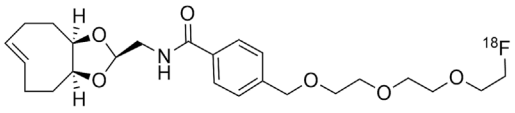

[^{18}F]MICA-212
[^{18}F]**16**

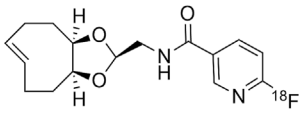

[^{18}F]MICA-213
[^{18}F]**17**

FIGURE 4 Structures[37] of d-TCOs, [^{18}F]**16** and [^{18}F]**17**.

mouse plasma, 86% and 79% of the parent compounds [^{18}F]**16** and [^{18}F]**17**, respectively, remained intact after the 2 h incubation.[37]

The promising in vitro stability led the authors to evaluate the pharmacokinetic profile of both d-TCOs in healthy female BALB/c mice through in vivo preclinical PET imaging. Both TCOs were seen to cross the BBB. The brain uptake of [^{18}F]**16** peaked after 15 min p.i. at 2.6 ± 0.1% ID/g, and its concentration remained stable over the first 60 min at 2.6 ± 0.5% ID/g. In comparison, the brain uptake of [^{18}F]**17** peaked after 10 min p.i. at 3.8 ± 1.7% ID/g, and by 60 min p.i, significant wash out was observed, and the concentration in the brain had decreased to 0.5 ± 0.1% ID/g. The stable brain concentration of [^{18}F]**16** was attributed to the presence of the PEG linker that was absent in [^{18}F]**17**.[37] Both tracers were excreted through a combination of hepatobiliary and renal clearance, and little defluorination was observed at 60 min p.i. Since both [^{18}F]**16** and [^{18}F]**17** showed favourable properties, the authors evaluated the kinetic performance of both TCOs making use of a model tetrazine. Stopped-flow kinetic analysis showed MICA-213 (**17**) had a tenfold higher rate constant in MeOH/H_2O (50:50) compared to MICA-212 (**16**) and was therefore selected for further evaluation in an in vivo preclinical PET pretargeted experiment. An anti-TAG72 mAb CC49 conjugated to a methyl tetrazine was injected into LS174T tumour-bearing mice. After 24 h, [^{18}F]**17** was administered to the mice. At 60 min p.i., the tumour was clearly visualised when compared to a control as shown in Figure 5. This was further confirmed with ex vivo biodistribution at 60 min p.i., which showed higher tumour uptake (1.36 ± 0.28% ID/g tissue) in LS174T tumour-bearing mice compared to the unmodified CC49 antibody control (0.78 ± 0.24% ID/g tissue).

2.1 | Other examples of radiolabelled TCOs

There are a few examples of radiolabelled TCOs that have not been investigated for their ability to cross the BBB.[38,39] Wang et al.[38] described the first reported radiolabelled *syn*-sTCO, [^{18}F]**21**, as seen in Scheme 6. The tosylate precursor was reacted with [^{18}F]TBAF in MeCN at 85°C for 10 min, to yield [^{18}F]**21** with a RCY of 29.3 ± 5.1%, a radiochemical purity of 99% and a molar activity of 2.1 ± 0.8 Ci/μmol (77.7 ± 29.6 GBq/μmol) after purification and formulation.

The stability of [^{18}F]**21** was investigated in both PBS and foetal bovine serum at 37°C. [^{18}F]**21** was found to be stable in PBS with 97.3% of the parent molecule remaining after 2 h of incubation and plasma stability of 74% after 1 h of incubation in foetal bovine serum. [^{18}F]**21** was not assessed in a pretargeted experiment but instead was used as prosthetic group to radiolabel a cyclic RGD peptide, cRGDyK, which bore a diphenyl-s-tetrazine (**22**), yielding [^{18}F]**23**, as seen in Scheme 7. [^{18}F]**23** was then imaged in U87MG tumour-bearing mice.[38] The addition of a PEG linker in coupling RGDyK to the tetrazine was found to improve the in vivo properties of the radioligand when compared to previous analogues explored by the group, and high tumour uptake was seen at 4 h p.i. at 8.9 ± 0.5% ID/g.[40,41] This led the authors to suggest that TCOs such as [^{18}F]**21** are useful prosthetic groups and should be considered when radiolabelling peptides and other large biomolecules going forward.[38]

Feng et al.[42] have also used [^{18}F]**21** to investigate a more hydrophilic tetrazine tagged peptide with the aim of increasing the tumour to background contrast for probes targeting non-small cell lung carcinoma.

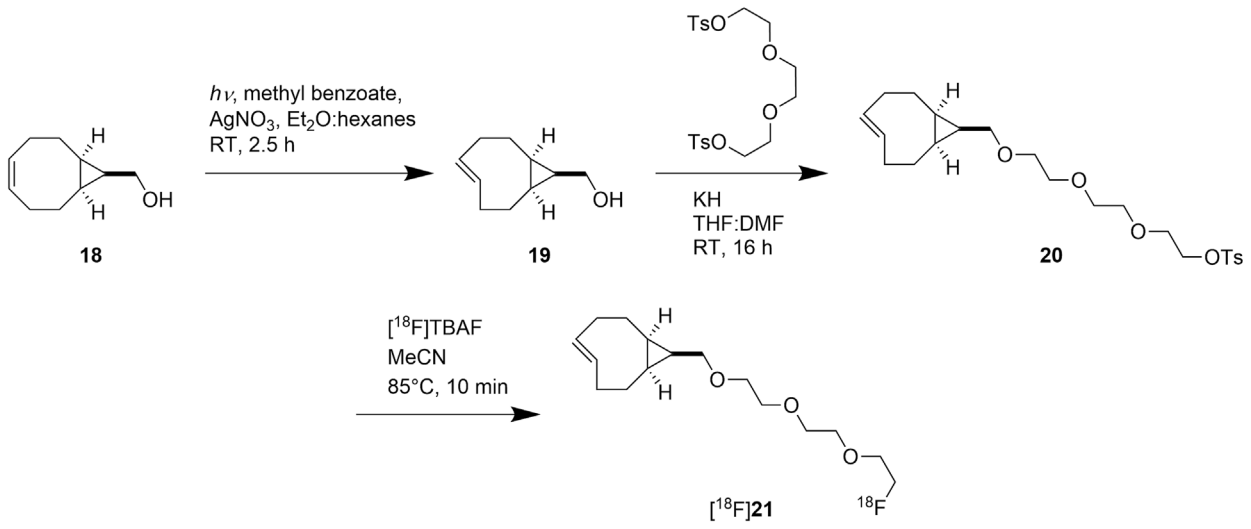

SCHEME 6 Precursor synthesis and radiochemical synthesis of TCO [^{18}F]**21**.

SCHEME 7 IEDDA reaction between [^{18}F]**21** and tetrazine tagged cyclic RGD peptide **22**.

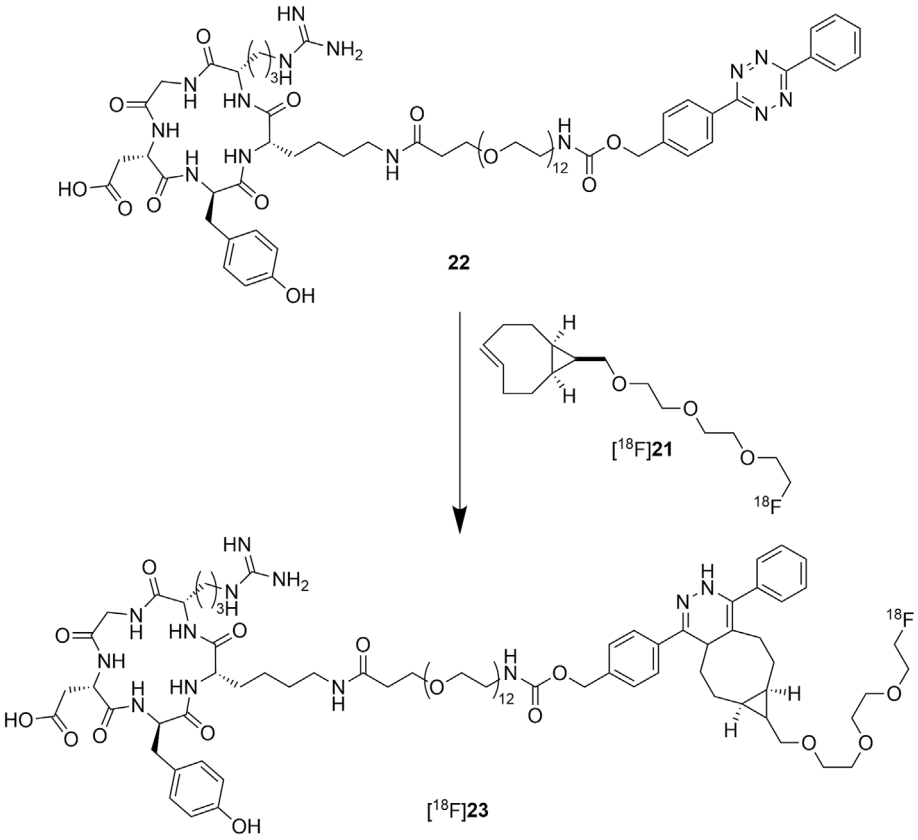

SCHEME 8 Radiochemical synthesis of [^{18}F]**25**.

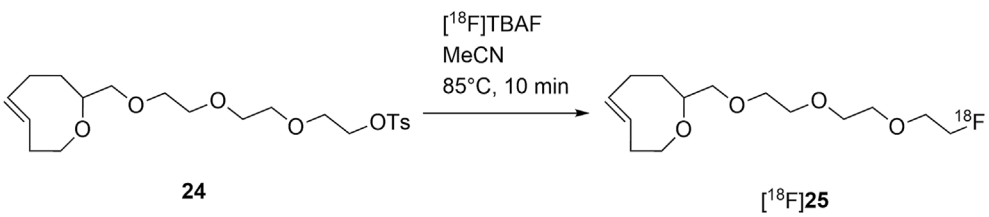

Wang et al.[39] then developed a radiolabelled TCO with a trans-5-oxocene TCO (oxoTCO) core, [^{18}F]**25**, and compared it to dTCO [^{18}F]**15**[35] and sTCO [^{18}F]**21**.[38] The tosylate oxoTCO precursor **24** was radiolabelled through a reaction with [^{18}F]TBAF in MeCN at 85°C for 10 min, as seen in Scheme 8. A modest RCY was achieved at 15 ± 1.9% with a radiochemical purity of >99%. The in vitro stability of [^{18}F]**25** was then assessed by radio-HPLC. After incubation in PBS for 1 h, 85.2% of the parent molecule was observed. The authors reported that this decrease in radiochemical stability was likely due to radiolysis.[39] The log *P* of [^{18}F]**25** was then evaluated in an octanol-water system and found to be 0.57 ± 0.02, suggesting that [^{18}F]**25** may not passively cross the BBB due to its high hydrophilicity. OxoTCO [^{18}F]**25** as well as dTCO [^{18}F]**15** and sTCO [^{18}F]**21** were used as prosthetic groups and clicked to a tetrazine conjugated to a neurotensin peptide, Lys-NT20.3. In vivo imaging of each clicked radioligand was performed in neurotensin receptor positive PC-3 tumour-bearing mice. The [^{18}F]oxoTCO-clicked radioligand was found to have a similar tumour uptake to the other click products but showed a much higher tumour to muscle ratio of 15.8 ± 2.2 at 30 min p.i., compared to 6.5 ± 1.5 and 3.8 ± 0.9 for the sTCO and dTCO, respectively. This high ratio was also sustained after 3.5 h at 16.2 ± 2.3.[39]

In an attempt to improve the stability of the TCO, Ruivo et al.[43] moved away from direct radiolabelling with fluorine-18, instead radiolabelling a TCO with aluminium [^{18}F]fluoride. To the best of our knowledge, this was the first example of such an application. [^{18}F]AlF was chelated to a TCO bearing a 1,4,7- triazacyclononane-1,-4,7-triacetic acid (NOTA) chelator, p-SCN-Bn-NOTA, giving [^{18}F]MICA-205, [^{18}F]**27** with a d.c. RCY of 12 ± 2.8% and radiochemical purity of ≥96%, seen in Scheme 9. The log*D* of [^{18}F]**27** was determined by the shake flask method and found to be 2.23 ± 0.01.

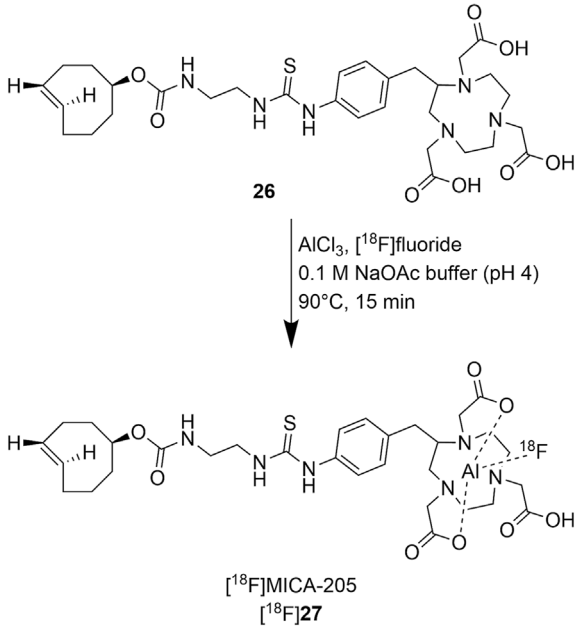

SCHEME 9 Radiosynthesis[43] of [^{18}F]**27**.

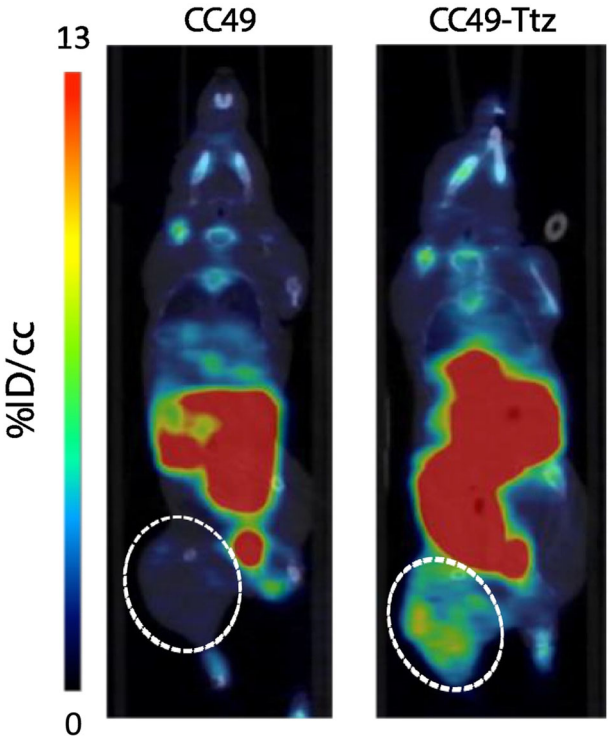

FIGURE 6 LS174T tumour-bearing mice were either pre-treated with an unmodified CC49 antibody (left) or a tetrazine tagged CC49 antibody (right) 24 h prior to administration of [^{18}F]**27**. Increased tumour uptake was observed in mice pre-treated with the tetrazine tagged CC49 antibody (right) as seen in the static image taken after 1 h p.i of [^{18}F]**27** above. Reproduced from Ruivo et al.[43] with permission from Elsevier.

In vitro stability of [^{18}F]**27** was assessed in saline at 37°C, with 90.3 ± 4.4% of the parent compound found intact after 2 h of incubation, with small amounts of isomerisation to the CCO observed.[43] With [^{18}F]**27** demonstrating promising in vitro stability, a biodistribution and metabolite study was performed in healthy BALB/c nude mice. At 15 min p.i., 67.7 ± 0.43% of the parent molecule remained intact in plasma, reducing to 51.9 ± 5.16% after 60 min p.i.[43] As expected, the major radiometabolite observed was the CCO. Due to the fast reaction kinetics of the IEDDA reaction, the authors postulated that [^{18}F]**27** will be consumed before isomerisation can occur; therefore, the in vivo performance of this radiolabelled TCO should be unaffected.[43] Biodistribution revealed that [^{18}F]**27** was excreted through both hepatobiliary and renal pathways with low bone uptake seen showing that the [^{18}F]aluminium fluoride complex was stable to defluorination. Poor blood clearance was also observed, reducing from 1.22 ± 0.18% ID/g at 15 min p.i. to 0.98 ± 0.59% ID/g at 60 min p.i., which could complicate in vivo PET image analysis due to high background. Finally, the authors investigated the performance of [^{18}F]**27** in a pretargeted preclinical PET experiment. LS174T tumour-bearing mice were initially treated with either an anti-TAG-72 mAb CC49 tagged with a methyl tetrazine previously developed by the group or an untagged anti-TAG-72 mAb CC49.[44] Following a 24 h pre-distribution period, [^{18}F]**27** was administered, and after 60 min, a static PET scan was performed (Figure 6). Visualisation of the tumour was only seen in mice treated with the CC49 tetrazine conjugate. This was confirmed through ex vivo biodistribution, which showed a tumour uptake of 0.67 ± 0.16% ID/g in mice treated with the CC49 tetrazine conjugate compared to 0.16 ± 0.08% ID/g for the untagged CC49 control.[43] Nevertheless, high accumulation of activity was present in the abdominal cavity, which could make quantification in this region difficult. Relatively low tumour uptake also needs to be improved for this radioligand to find further use.

More recently, an undisclosed novel TCO scaffold was explored by Adhikari et al.[45] and reported in a conference abstract. From a library of fluorinated d-TCOs, a promising d-TCO was identified and radiolabelled. The d-TCO was radiolabelled from a tosylate precursor using [^{18}F]fluoride in dimethylformamide (DMF) at 100°C for 10 min yielding the [^{18}F]d-TCO with a d.c RCY of 5.5% from EOB and radiochemical purity of >98%. Lipophilicity was assessed through the shake flask method, which gave a log *D* of 0.59 ± 0.07, suggesting that the [^{18}F]d-TCO would be less likely to pass the BBB. Finally, the plasma stability of the radiolabelled TCO was assessed in mouse plasma with approximately 30% of the parent molecule observed after a 2-h incubation period.[45]

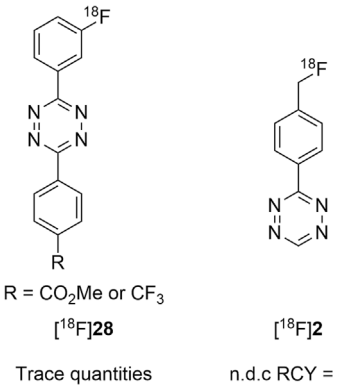

FIGURE 7 Structures[32] of the first reported tetrazines radiolabelled with fluorine-18, [^{18}F]**28** and [^{18}F]**2**.

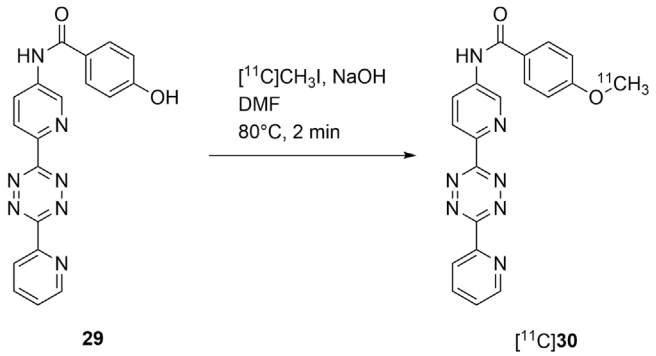

SCHEME 10 Radiochemical synthesis of [^{11}C]**30**, first reported by Herth et al.[47]

2.2 | Radiolabelled tetrazines

As mentioned above, Li et al.[32] reported the first radiolabelled tetrazine, [^{18}F]**2** (Figure 7). Initially, attempts were made to radiolabel a 3,6-diaryl-tetrazine using nucleophilic aromatic substitution from the corresponding nitro precursor using either [^{18}F]KF•K*222*®•K_2CO_3 or [^{18}F]TBAF•$TBAHCO_3$; however, only trace quantities of [^{18}F]**28** were observed. Radiolabelling was then attempted on a mono-aryl tetrazine bearing a mesylate at the benzylic position. The mesylate precursor was reacted with [^{18}F]TBAF at 85°C for 15 min and gave [^{18}F]**2** in a non-decay corrected RCY (n.d.c RCY) of ~1%.[32]

The above highlighted the poor stability of the tetrazine core under typical S_N2 nucleophilic substitution conditions with [^{18}F]fluoride, that is, prolonged heating under basic conditions, and thus represents the biggest challenge in radiolabelling tetrazines.[19,32,46] More recently, Bratteby et al.[46] have reported a method for the radiolabelling of base sensitive tetrazines using polyanionic preconditioning agents for the quaternary ammonium ion exchange cartridges used for [^{18}F]fluoride trapping and weak bases as [^{18}F]fluoride eluents. Under these conditions, radiolabelled tetrazines that were prepared in low RCY using 'standard' [^{18}F]fluoride preparation conditions were successfully radiolabelled in up to 23% RCY, offering a new route to ^{18}F- radiolabelled tetrazines that were previously inaccessible.

2.3 | Brain penetrant tetrazines

In 2013, Herth et al.[47] reported the synthesis of a carbon-11 radiolabelled tetrazine, [^{11}C]**30**, as seen in Scheme 10. The phenol precursor **29** was methylated with [^{11}C]MeI in tetrahydrofuran, with NaOH as a base, at 80°C over 2 min. Tetrazine [^{11}C]**30** was isolated with a d.c. RCY of 33 ± 5% (n = 5) from EOS, a radiochemical purity of >98% and molar activity of 40–80 GBq/μmol in a total time of 60 min. The log$D$ of [^{11}C]**30** was determined by ultra-high performance liquid chromatography and found to be 3.37.

The in vivo properties of [^{11}C]**30** were not investigated until 2019 by Steèn et al.[48] The occasional formation of a suspected radiolysis impurity in the synthesis performed by Herth et al. led Steèn et al. to modify the radiosynthesis of [^{11}C]**30**. Through the replacement of MeCN with EtOH in the HPLC eluent, a molar activity of 50–350 GBq/μmol was achieved whilst maintaining the radiochemical purity of >97%.[49,50] The group then investigated the in vitro and in vivo properties of [^{11}C]**30** in both mice and pigs. A pretargeted experiment was explored, whereby a TCO-tagged polyglutamic acid was directly administered into the tumour of CT26 tumour-bearing BALB/c mice. After 60 min, [^{11}C]**30** was administered to the mice, and preclinical PET scans were performed. No specific tumour uptake was observed, and high radioactivity uptake was observed in the liver and bladder. The authors hypothesised that the highly reactive bis-pyridyl tetrazine core was unstable in vivo and therefore unable to react with the pre-injected TCO. Stability studies in mice confirmed that [^{11}C]**30** had poor in vivo stability with just 47% of intact [^{11}C]**30** observed after 1 min p.i. by radio-HPLC, decreasing to 27% after 5 min. With potential applications of the IEDDA in the brain in mind, the group also investigated whether [^{11}C]**30** was able to cross the BBB in both mice and pigs. In mice, brain uptake was observed, but it was unclear if this was the parent molecule [^{11}C]**30** or a radiometabolite. Not deterred by this result, and encouraged by the observation of interspecies differences in BBB transport, [^{11}C]**30** was then investigated in pigs.[51] In pigs, brain uptake was observed, with a peak SUV in the range of 2.5–3, followed by fast washout. [^{11}C]**30** was also found to be metabolised in pigs although degradation

was much slower over the initial 10 min period. Further studies are therefore required to elucidate if [^{11}C]**30** has promise for pretargeted imaging within the brain. There is also a need to establish if BBB penetrative metabolites are responsible for the observed brain uptake seen in mice.

Karver et al.[14] evaluated the reactivity, stability and solubility of 12 tetrazines, as seen in Table 1. Initially, the reaction kinetics of each tetrazine was evaluated against a norbornane, ((1*S*,2*S*,4*S*)-bicyclo[2.2.1]hept-5-en-2-ylacetic acid) at 37°C. Second-order rate constants were calculated from pseudo-first order rate constants, highlighting that tetrazines bearing stronger electron withdrawing groups, such as **34**, demonstrated the fastest reaction kinetics. H-tetrazines were also found to display faster reaction kinetics than expected. Therefore, factors such as steric hindrance were also suggested to influence the rate of reaction. The stability of each tetrazine was then evaluated after 14 h of incubation in PBS (pH 7.4) at 37°C. As expected, tetrazines bearing stronger electron withdrawing groups were less stable than their more electron-rich counterparts. The most promising tetrazines, **31–39**, were then further evaluated. A stopped-flow spectrophotometer was used to assess the reaction kinetics of the remaining tetrazines against a TCO in PBS at pH 7.4 at 37°C, a more relevant dienophile for pretargeted imaging. Tetrazine **39** demonstrated the fastest reaction kinetics, displaying a second order rate constant of 30,000 ± 3,000 M^{-1} s^{-1}, outperforming **31**, **33**, **34** and **38**, which had faster reaction kinetics when reacted with the norbornane. Steric hindrance was again suggested as the potential cause for this observation. Stability in foetal bovine serum at 37°C was then assessed after a 10 h incubation period. This identified that more electron-rich tetrazines had greater stability. The authors concluded that H-tetrazines displayed the best balance between reactivity, stability and solubility.

Drawing the experience of Karver et al.,[14] Denk et al.[52] developed [^{18}F]**45** as seen in Scheme 11. First, the authors assessed the plasma stability of **45** with 99% of the parent molecule observed after 12 h of incubation at 37°C. Encouraged by this promising plasma stability, [^{18}F]**45** was radiolabelled from a tosylate precursor, **46**, with [^{18}F]KF•K*222*®•K_2CO_3 in MeCN at 90°C for 5 min,

TABLE 1 Structures of the 12 tetrazines evaluated by Karver et al.[14]

Tetrazine Core	Tetrazine number	R^1	R^2
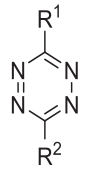	**31**	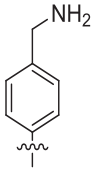	H
	32		Me
	33		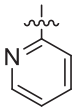
	34		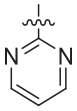
	35	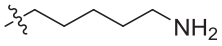	H
	36		Me
	37		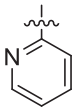
	38		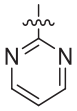
	39	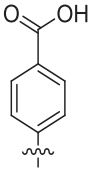	H
	40		Me
	41		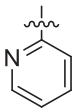
	42		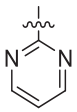

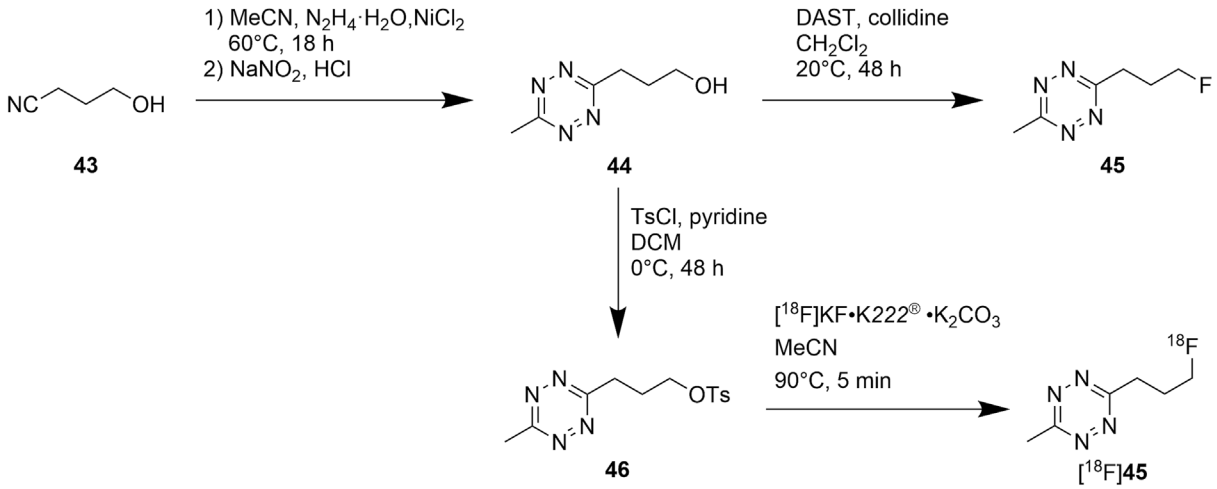

SCHEME 11 Synthesis of radiochemical precursor **46** and reference standard **45,** and radiochemical synthesis[52] of [^{18}F]**45**.

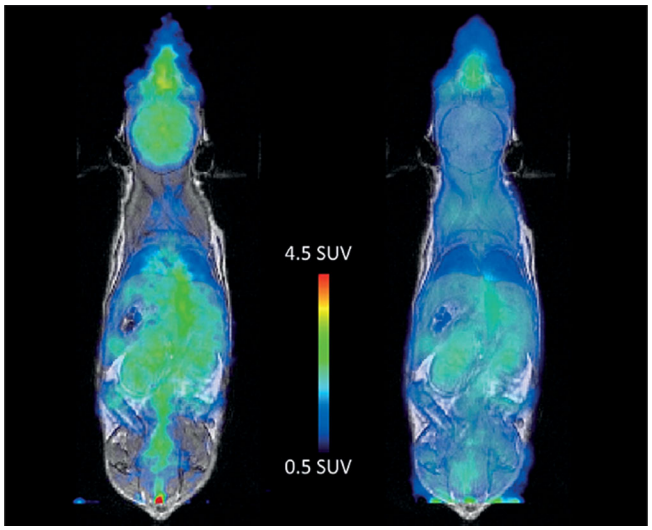

FIGURE 8 Summed PET/MRI images from 0–5 min (left) and 5–120 min (right) confirming that [^{18}F]**45** was able to cross the BBB in BALB/c mice. Reproduced from Denk et al.[52] with permission from Wiley.

affording [^{18}F]**45** with d.c. RCY of 16 ± 2%. The synthesis was then automated giving [^{18}F]**45** in d.c. RCY of 5.2%, although this procedure was not optimised.

In vivo dynamic preclinical PET scans were performed in female BALB/c mice and confirmed that [^{18}F]**45** was able to cross the BBB with a peak SUV of ~3 after 2 min, as shown in Figure 8.[45,52] Upon completion of the preclinical PET scan (120 min), mouse plasma was analysed by radio-TLC, to assess the metabolic stability of [^{18}F]**45**. Approximately 85% of the parent molecule was observed, showing that [^{18}F]**45** possessed good in vivo mouse plasma stability. To explore the reactivity of [^{18}F]**45** further, in vivo experiments were performed in female BABL/c mice. [^{18}F]**45** was initially administered to the mice, and after 20 min, an sTCO was administered. At selected time points, blood samples were drawn from the mice. To prevent tetrazine [^{18}F]**45** from reacting further with the sTCO during analysis, excess sTCO was sequestered with a more reactive mono aryl tetrazine. Unreacted [^{18}F]**45** was quantified by radio-TLC, and [^{18}F]**45** was found to be completely consumed within 30 min.

Continuing with their research, Denk et al.[53] then radiolabelled a low molecular weight tetrazine with carbon-11. The precursor was synthesised over two steps to give a free amine, **48**. This was methylated with [^{11}C] methyl triflate at 75°C for 5 min in MeCN to afford [^{11}C]**49**, seen in Scheme 12. [^{11}C]**49** was synthesised with a d.c. RCY of 52 ± 6% and a radiochemical purity of >95% in a total synthesis time of 30 min.

The biodistribution of [^{11}C]**50** was investigated in female BALB/c mice in preclinical PET/MR scans over 60 min, and following completion of the scan, ex vivo biodistribution was performed. [^{11}C]**50** was able to cross the BBB with high uptake observed in the brain within the first 5 min. Ex vivo biodistribution confirmed that [^{11}C]**50** crossed the BBB with an SUV of 1–1.5 observed after 60 min p.i.[53] The in vivo stability of [^{11}C]**50** was then explored in both plasma and urine as [^{11}C]**50** was excreted through the renal pathway. In urine, 50% of the parent molecule was seen after 60 min p.i, whereas in plasma, [^{11}C]**50** was metabolised more quickly, with only 38% of the parent molecule seen at the same time point, determined by radio-TLC. In both urine and plasma, two main metabolites were observed. The group then explored [^{11}C]**50** in vivo click capabilities in female BALB/c mice. Initially, an s-TCO was administered to the mice. After 5 min, [^{11}C]**50** was administered. Blood was then analysed and showed that after 5 min, 98% of

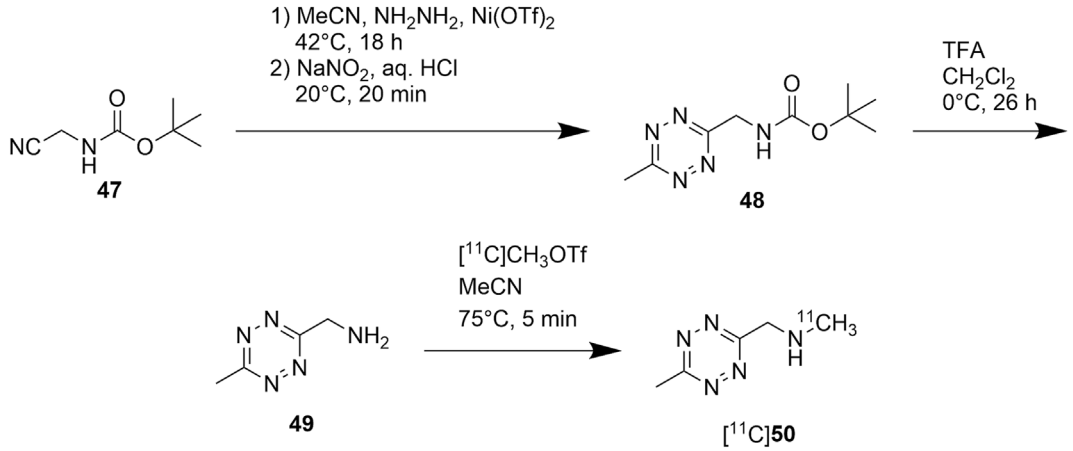

SCHEME 12 Synthesis[53] of radiochemical precursor **49** and radiosynthesis of [^{11}C]**50**.

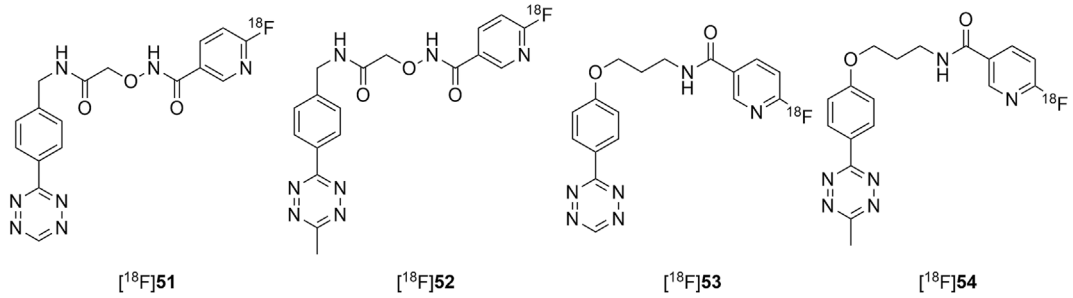

FIGURE 9 Structures of the four tetrazines [^{18}F]**51–54** synthesised by Schlein et al.[54] for use in pretargeted imaging of amyloid beta.

[^{11}C]**50** had been converted to the clicked product. This then led to the investigation of [^{11}C]**50** in a pretargeted experiment. Mesoporous silica nanoparticles, which were known to accumulate in the lungs, were tagged with either TCOs or s-TCOs and administered to female BALB/c mice. After 5 min, [^{11}C]**50** was administered to the mice. When compared to the biodistribution of [^{11}C]**50**, a threefold increase in activity concentration in the lungs was observed when mice were pretreated with the TCO nanoparticles. TCO-nanoparticles also outperformed the more reactive s-TCO-nanoparticles, which was attributed to poorer in vivo stability of s-TCOs. This highlighted the fine balance between reactivity and stability and reiterates the importance of the careful consideration of the properties of tetrazines and TCOs when selecting the reactive handle conjugated to the targeting molecule.[53]

In a conference abstract, Schlein et al.[54] reported the synthesis of four ^{18}F-radiolabelled tetrazines for use in pretargeted imaging of amyloid-beta. First 6-[^{18}F]fluoronicotinic acid tetrafluorophenyl ester was synthesised on a solid support and then coupled to amine or aminooxy bearing tetrazines to give [^{18}F]**51-54** as seen in Figure 9. The tetrazines were synthesised with radiochemical purities of >93% and in radioactivity yields (590 ± 330 MBq) suitable for preclinical PET scans in both transgenic (tg-ArcSwe) and wild-type mice. Each tetrazine was able to cross with BBB with peak SUVs between 1.5 and 2 decreasing to 0.29–0.59 at 60 min p.i. for the methyl-tetrazines, [^{18}F]**52** and [^{18}F]**54**.[54] Further evaluation is currently underway in order to assess how effective these tetrazines are for use in pretargeted imaging.

2.4 | Attempts at pretargeted imaging of the brain

Shalgunov et al.[55] reported the synthesis of a library of 18 tetrazines based on a 3-fluorophenyltetrazine core, exploring whether calculated physiochemical properties could be used as predictors for improving the performance of tetrazines for pre-targeted imaging within the brain. Various parameters (clogP, clog$D_{7.4}$, topological polar surface area, central nervous system multiparameter optimization scores and BBB scores) were calculated for each tetrazine.[24,56] All 18 tetrazines were radiolabelled with fluorine-18 from the corresponding stannane precursors through copper-mediated

SCHEME 13 Radiochemical synthesis of [^{18}F]**56** using a copper-mediated radiofluorination as reported by Shalgunov et al.[55] In some cases, the precursor contained a protecting group which was removed after the radiolabelling step with trifluoroacetic acid at 70°C for 10 min.

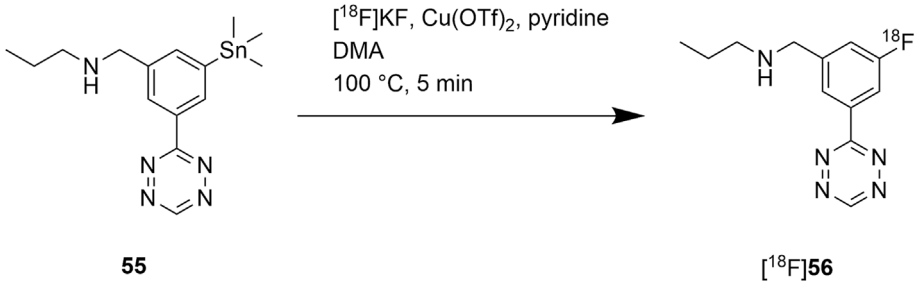

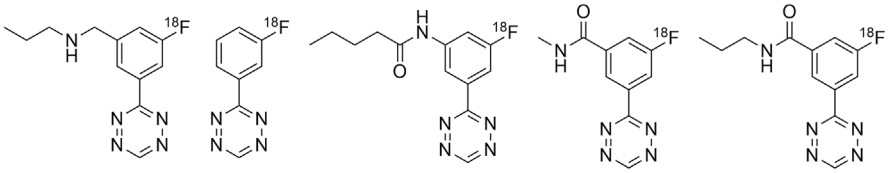

	[^{18}F]**56**	[^{18}F]**57**	[^{18}F]**58**	[^{18}F]**59**	[^{18}F]**60**
Peak Uptake (%ID/mL)	0.86	0.78	0.77	0.68	0.95
In vivo contrast (Cor/Cer)	1.09	0.89	0.90	1.59	1.07
Washout (min^{-1})	0.0398	0.0201	0.0823	0.0431	0.0649

FIGURE 10 Structures of tetrazines [^{18}F]**56–60**, chosen for further in vivo evaluation. Peak uptake, in vivo image contrast (cortex (Cor) to cerebellum (Cer) ratio determined from autoradiography) and washout (quantified as peak uptake/area under the curve) provided a criteria for further analysis.[55]

radiofluorination as seen in Scheme 13. All 18 tetrazines were synthesised in d.c RCYs in the range of 9–19%, radiochemical purities of >92% and molar activities of 70-210 GBq/μmol. Fifteen of the radiolabelled tetrazines underwent further evaluation, whilst the remaining three were found to be unstable in the formulation buffer.

The radiolabelled tetrazines were assessed for their performance in pretargeted imaging using a combination of in vitro autoradiography and in vivo dynamic PET scans. Autoradiography experiments were performed with brain sections from amyloid-beta (Aβ) expressing Tg-ArcSwe mice, which were pre-treated with an anti-Aβ TCO-bearing antibody. Each tetrazine was evaluated and ranked according to the contrast between a high Aβ expressing area (cortex) and low Aβ expressing area (cerebellum). Dynamic PET scans were performed with healthy Long Evans rats. The ratio of peak uptake and area under the curve from time activity curves was used as a proxy to evaluate the washout of each tetrazine. From the tetrazines examined, [^{18}F]**58**, [^{18}F]**59** and [^{18}F]**60** were the highest ranking, whilst [^{18}F]**57** was the worst performing tetrazine. As such, these were selected for further in vivo click evaluation, along with [^{18}F]**56**, which was selected to represent tetrazines, which had intermediate performance. The selected tetrazines are shown in Figure 10.

In a proof-of-concept experiment to explore whether these radiolabelled tetrazines, [^{18}F]**56–60**, would successfully undergo an in vivo click reaction, the right striatum of Long-Evans rats was injected with TCO-tagged PeptoBrush polymer, before each of the selected ^{18}F-labelled tetrazines were administered to the rats. All five tetrazines accumulated in the right striatum at the point of PeptoBrush injection, as shown for [^{18}F]**56** in Figure 11, suggesting that the in vivo click reaction was successful with all the examined tetrazines. The group examined the relative contrast (*ratio* of uptake in treated right striatum to uptake in untreated left striatum) and absolute contrast (*difference* of uptake in treated right striatum to uptake in untreated left striatum) as key

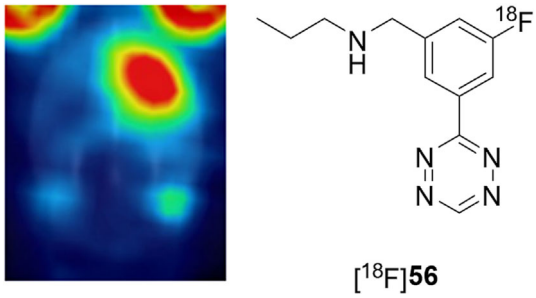

FIGURE 11 In vivo PET image of [^{18}F]**56** showing that [^{18}F]**56** was successfully clicked to the TCO-tagged PeptoBrush in the right striatum, with minimal uptake in the untreated left striatum. Reproduced from V. Shalgunov et al.,[55] with permission from the Royal Society of Chemistry.

parameters for assessment. Unexpectedly, this showed that [^{18}F]**56** and [^{18}F]**57** outperformed the predicted best tetrazines from the first round of evaluation, with [^{18}F]**56** found to show the optimal combination of relative and absolute contrast of all the radiolabelled tetrazines assessed.

Finally, the in vivo metabolism of each tetrazine was assessed after 90 min. [^{18}F]**58** and [^{18}F]**60** showed poor stability with, 5% of the parent molecule observed. [^{18}F]**56** showed improved stability, with 30% of the parent observed. [^{18}F]**57** and [^{18}F]**59** had the greatest stability, with 50% of the parent molecule recovered. Hydrophilic metabolites were seen in all tetrazines but were not expected to cross the BBB. The authors concluded that [^{18}F]**56** showed the best balance of properties for pre-targeted imaging, which would not have been predicted by their initial model, highlighting the value of in vivo evaluation of novel tetrazines. Ultimately, the group has described a useful model for further assessing radiolabelled tetrazines for in vivo pre-targeting applications.

One of the first attempts at pretargeted imaging of the brain was reported by Cook et al.[57] An absorption, distribution, metabolism and excretion (ADME) study led to the identification of F-537-Tz, **61** as a promising tetrazine for pre-targeted imaging in the brain. The metabolic profile of **61** was assessed by mass spectrometry in hepatocytes from rat, cynomolgus monkeys and human cell lines. Two major metabolites were observed, the reduced dihydrotetrazine, **62** and an oxadiazole derivative, which was thought to occur through oxidation of the dihydrotetrazine intermediate to form **63** as seen in Scheme 14.

However, as the two metabolites are unable to react with TCOs, **61** was taken forward and radiolabelled with fluorine-18. First, [^{18}F]fluoroethyl azide was synthesised from a tosylate precursor, **64** reacting with [^{18}F]KF•*K222*®•K_2CO_3 in MeCN at 105°C for 5 min, before being reduced to the amine [^{18}F]**66** with triphenylphosphine in DMF at 80°C for 15 min. The amine, [^{18}F]**66**, was then reacted with the NHS ester of 2-(4-[1,2,4,5-tetrazin-3-yl]phenyl)acetic acid at 37°C for 12 min, to give [^{18}F]F-537-Tz ([^{18}F]**61**), seen in Scheme 15. [^{18}F]**61** was synthesised with d.c. RCY of 6% and radiochemical purity of >95% in a total time of 100 min.

The aim of the study was to develop a radiolabelled tetrazine, which was able to explore the biodistribution

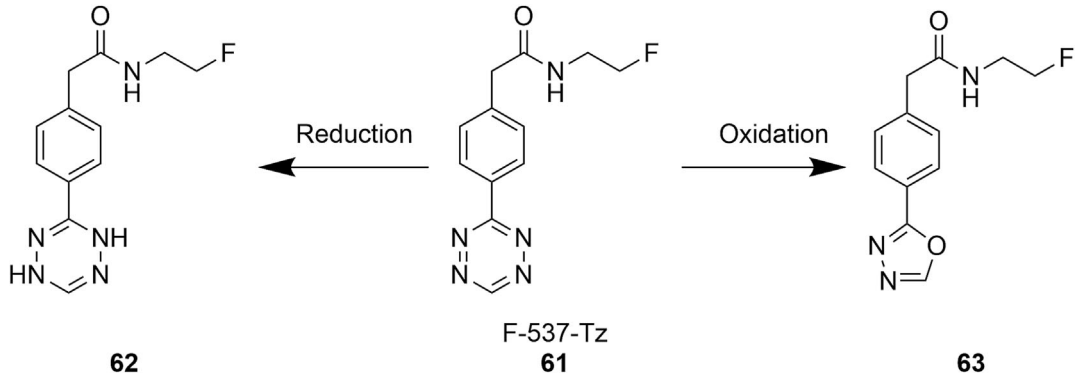

SCHEME 14 The two major metabolites were identified through either reduction, **62** or oxidation, **63** of the parent molecule and **61** in vitro.

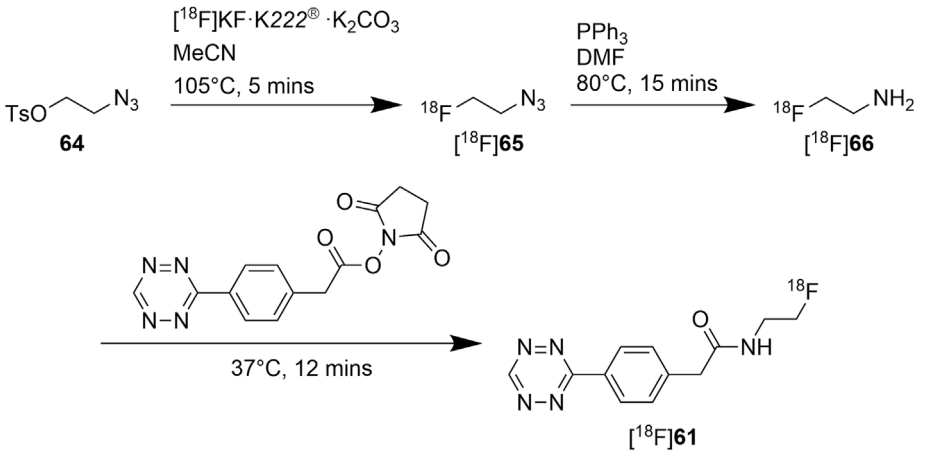

SCHEME 15 Radiosynthesis[57] of [^{18}F]**61** via the intermediate [^{18}F]2-fluoroethylamine [^{18}F]**66**.

of antisense oligonucleotides (ASOs) post administration. As a model, an ASO targeting Malat1 (a highly conserved target with high CNS expression) was coupled to a TCO via a linker, and both the tetrazine and TCO were investigated for their in vitro and in vivo properties such as stability, cell uptake and specific binding. In vitro autoradiography was performed, whereby Sprague–Dawley (SD) rats were intrathecally dosed with the TCO-tagged Malat1 ASO to bypass the BBB. The rats were sacrificed 24 h later and brains sectioned, and tissue slices were then incubated with either [^{18}F]**61** or a 250-fold excess of **61**, followed by [^{18}F]**61**. The highest accumulation of radioactivity was observed in the meninges around the brain, with some binding also observed in the cortical regions. Pretreatment with **61** confirmed that binding was specific. The pharmacokinetics of [^{18}F]**61** was then assessed in naïve SD rats confirming brain uptake, but this identified that [^{18}F]**61** was slow to washout of the brain, an unfavourable property, which can reduce image contrast.

Nevertheless, the authors were able to show that in rats that were intrathecally pre-administered with different doses of Malat1 ASO, a dose dependent increase in uptake was observed after administration of [^{18}F]**61**. The results in rats led the authors to explore both the ^{18}F-labelled tetrazine and TCO-tagged Malat1 ASO in non-human primates (NHP). Slower washout of [^{18}F]**61** from the brain was observed in the NHP compared to rats. Furthermore, the poor washout of [^{18}F]**61** led to inadequate image contrast when tested in a pre-targeted experiment, where, despite intrathecal pre-treatment with the Malat-1 ASO, no statistically significant increase in uptake of the radiotracer was observed in the brain. This led to the conclusion that the in vivo properties of [^{18}F]**61** were unsuitable for transition to the clinical setting as slow brain clearance impacted the contrast of the PET image. This study does however provide the first steps into pretargeted imaging within the brain.

3 | CONCLUSIONS AND FUTURE OUTLOOK

PET imaging of pathology in the brain has largely relied on the use of small lipid soluble ligands, which passively diffuse across the BBB or polar molecules that mimic endogenous molecules and exploit active transport systems to cross the BBB. Pretargeting has the potential to greatly expand the scope of PET imaging agents available for interrogation of diseases that affect the brain, and as described above, this has largely focussed on the IEDAA reaction between activated tetrazines and TCOs.[2,19,58] Pretargeting efforts in the oncology space are now reaching clinical trial stage in humans[59,60]; however, we are still waiting to see similar successes with pretargeting in the brain. There is an abundance of potential targets in the brain that have remained intractable or very challenging to develop radiotracers for using small-molecule based PET probes (e.g., alpha-synuclein,[61] Huntingtin[62,63] and AMPA receptors[64]). Imaging these targets using a pretargeting approach with selective and specific monoclonal antibodies or antibody fragments would greatly facilitate understanding of both the healthy and diseased brain. Towards this goal, the focus has been the preparation of tetrazines and TCOs, which are able to cross the BBB. Perhaps unexpectedly, it has proven challenging to find either a TCO or a tetrazine labelled with either fluorine-18 or carbon-11, which displays all the desirable properties required of such an agent for imaging in pretargeting, including

- Good chemical (and radiolytic) stability
- Good in vivo stability
- Lack of formation of BBB penetrant metabolites
- Fast reaction kinetics
- High radiochemical yielding, simple synthesis
- High initial brain uptake and fast washout

Recent developments in understanding the drivers of reactivity and stability of tetrazines, as well as the development of more mild reaction conditions for the ^{18}F-radiolabelling of tetrazines, will spur the development of new radiolabelled tetrazines.[15,46] These new tetrazines would be expected to show superior properties (e.g., RCY and in vivo stability) to those that have already been studied. Shalgunov et al.[55] have recently reported tetrazine [^{18}F]**56**, which shows many of these ideal properties. The same group has also recently reported the determination of the minimum concentration of TCO-labelled antibodies required for successful pretargeting in the brain and showed that this concentration can be achieved using antibodies transported across the BBB using the transferrin receptor.[65] The community eagerly awaits further validation of their system in a more complex, disease relevant pretargeting model.

PET radiochemists are well suited for the radiolabelling and preliminary evaluation of radiolabelled TCOs and tetrazines for pre-targeting imaging in the brain. However, this still leaves a gap to find suitable methods for transporting large biomolecules (e.g., antibodies or ASOs) across the BBB. To date, those applied for PET imaging have exploited direct injection of a reactive TCO into the brain for validation of the reactivity of ^{18}F-labelled tetrazines or direct injection of the TCO-targeting fragment into the cerebrospinal fluid as described in the last example discussed above.[55,57] Other

approaches for PET imaging with radiolabelled antibodies or antibody fragments in the brain have used receptor mediated transcytosis (RMT) and the transferrin receptor shuttle system to transport a bifunctional antibody, targeted to the transferrin receptor and amyloid-beta, or smaller bifunctional Tribodies across the BBB.[66,67] This approach has not as yet been applied to pre-targeted PET imaging in the brain.

Over the last 5 years, there has been increased focus on using pretargeted PET imaging in the brain, and it appears that the imaging tools are now reaching the stage where they show favourable in vivo properties. From the examples described above, there is still no simple, well-tested, generally applicable tool to transport large biomolecules across the BBB in amounts suitable for PET imaging. Even well-explored systems like the transferrin shuttle require significant optimization of conditions to work well in the PET imaging context.[68] Without a general protocol, researchers are still required to optimise each case individually. There are many methods for transporting biological molecules into the brain, which are yet to be applied to pretargeted PET imaging, and several excellent reviews offer many opportunities for exploration of this paradigm.[3–9] In the near future, the use of pretargeted PET imaging will no doubt revolutionise the imaging of targets in the brain, which have thus far proven challenging to image using small molecule ligands, and with the rapid growth of publications in this area, it appears to be only a matter of time before this approach becomes common practice.

CONFLICT OF INTEREST STATEMENT

The authors have no conflicts of interest to declare.

DATA AVAILABILITY STATEMENT

Data sharing not applicable - no new data generated.

ORCID

Stephen Thompson https://orcid.org/0000-0003-3596-7812
Selena Milicevic Sephton https://orcid.org/0000-0002-1105-6726

REFERENCES

1. Ametamey SM, Honer M, Schubiger PA. Molecular imaging with PET. *Chem Rev*. 2008;108(5):1501-1516. doi:10.1021/cr0782426
2. Stéen EJL, Edem PE, Nørregaard K, et al. Pretargeting in nuclear imaging and radionuclide therapy: improving efficacy of theranostics and nanomedicines. *Biomaterials*. 2018;179:209-245. doi:10.1016/j.biomaterials.2018.06.021
3. van den Broek SL, Shalgunov V, Herth MM. Transport of nanomedicines across the blood–brain barrier: challenges and opportunities for imaging and therapy. *Biomater Adv*. 2022;141:213125. doi:10.1016/j.bioadv.2022.213125
4. Nance E, Pun SH, Saigal R, Sellers DL. Drug delivery to the central nervous system. *Nat Rev Mater*. 2021;7(4):314-331. doi:10.1038/s41578-021-00394-w
5. Pardridge WM. Drug transport across the blood–brain barrier. *J Cereb Blood Flow Metab*. 2012;32(11):1959-1972. doi:10.1038/jcbfm.2012.126
6. Pardridge WM. A historical review of brain drug delivery. *Pharmaceutics*. 2022;14(6):1283. doi:10.3390/pharmaceutics14061283
7. Oller-Salvia B, Sánchez-Navarro M, Giralt E, Teixidó M. Blood–brain barrier shuttle peptides: an emerging paradigm for brain delivery. *Chem Soc Rev*. 2016;45(17):4690-4707. doi:10.1039/C6CS00076B
8. Sánchez-Navarro M, Giralt E, Teixidó M. Blood–brain barrier peptide shuttles. *Curr Opin Chem Biol*. 2017;38:134-140. doi:10.1016/j.cbpa.2017.04.019
9. Oswald M, Geissler S, Goepferich A. Targeting the central nervous system (CNS): a review of rabies virus-targeting strategies. *Mol Pharm*. 2017;14(7):2177-2196. doi:10.1021/acs.molpharmaceut.7b00158
10. Lossouarn A, Renard PY, Sabot C. Tailored bioorthogonal and bioconjugate chemistry: a source of inspiration for developing kinetic target-guided synthesis strategies. *Bioconjug Chem*. 2021;32(1):63-72. doi:10.1021/acs.bioconjchem.0c00568
11. Dube DH, Bertozzi CR. Metabolic oligosaccharide engineering as a tool for glycobiology. *Curr Opin Chem Biol*. 2003;7(5):616-625. doi:10.1016/j.cbpa.2003.08.006
12. Png ZM, Zeng H, Ye Q, Xu J. Inverse-electron-demand Diels–Alder reactions: principles and applications. *Chem - An Asian J*. 2017;12(17):2142-2159. doi:10.1002/asia.201700442
13. Oliveira BL, Guo Z, Bernardes GJL. Inverse electron demand Diels–Alder reactions in chemical biology. *Chem Soc Rev*. 2017;46(16):4895-4950. doi:10.1039/C7CS00184C
14. Karver MR, Weissleder R, Hilderbrand SA. Synthesis and evaluation of a series of 1,2,4,5-Tetrazines for bioorthogonal conjugation. *Bioconjug Chem*. 2011;22(11):2263-2270. doi:10.1021/bc200295y
15. Svatunek D, Wilkovitsch M, Hartmann L, Houk KN, Mikula H. Uncovering the key role of distortion in bioorthogonal tetrazine tools that defy the reactivity/stability trade-off. *J am Chem Soc*. 2022;144(18):8171-8177. doi:10.1021/jacs.2c01056
16. Taylor MT, Blackman ML, Dmitrenko O, Fox JM. Design and synthesis of highly reactive dienophiles for the tetrazine-trans-cyclooctene ligation. *J am Chem Soc*. 2011;133(25):9646-9649. doi:10.1021/ja201844c
17. Darko A, Wallace S, Dmitrenko O, et al. Conformationally strained trans-cyclooctene with improved stability and excellent reactivity in tetrazine ligation. *Chem Sci*. 2014;5(10):3770-3776. doi:10.1039/C4SC01348D
18. Lambert WD, Scinto SL, Dmitrenko O, et al. Computationally guided discovery of a reactive, hydrophilic trans-5-oxocene dienophile for bioorthogonal labeling. *Org Biomol Chem*. 2017;15(31):6640-6644. doi:10.1039/C7OB01707C
19. García-Vázquez R, Battisti U, Herth M. Recent advances in the development of tetrazine ligation tools for pretargeted nuclear

imaging. *Pharmaceuticals*. 2022;15(6):685. doi:10.3390/ph15060685
20. Tolshchina SG, Rusinov GL, Charushin VN. 1,2,4,5-tetrazines and azolo[1,2,4,5]tetrazines: synthesis and reactions with nucleophiles. *Chem Heterocycl Compd*. 2013;49(1):66-91. doi:10.1007/s10593-013-1232-2
21. Otaru S, Niemikoski H, Sarparanta M, et al. Metabolism of a bioorthogonal PET tracer candidate [19 F/18 F]SiFA-tetrazine in mouse liver microsomes: biotransformation pathways and defluorination investigated by UHPLC-HRMS. *Mol Pharm*. 2020;17:3115.
22. Wyffels L, Thomae D, Waldron A-M, et al. In vivo evaluation of 18F-labeled TCO for pre-targeted PET imaging in the brain. *Nucl Med Biol*. 2014;41(6):513-523. doi:10.1016/j.nucmedbio.2014.03.023
23. Rossin R, van den Bosch SM, ten Hoeve W, et al. Highly reactive trans-cyclooctene tags with improved stability for Diels–Alder chemistry in living systems. *Bioconjug Chem*. 2013;24(7):1210-1217. doi:10.1021/bc400153y
24. Wager TT, Hou X, Verhoest PR, Villalobos A. Moving beyond rules: the development of a central nervous system multiparameter optimization (CNS MPO) approach to enable alignment of druglike properties. *ACS Chem Nerosci*. 2010;1(6):435-449. doi:10.1021/cn100008c
25. Barbet J, Bardiès M, Bourgeois M, et al. Radiolabeled antibodies for cancer imaging and therapy. In: *Methods in molecular biology*. Humana Press Inc.; 2012:681-697.
26. Kraeber-Bodéré F, Bodet-Milin C, Rousseau C, et al. Radioimmunoconjugates for the treatment of cancer. *Semin Oncol*. 2014;41(5):613-622. doi:10.1053/j.seminoncol.2014.07.004
27. Martins CD, Kramer-Marek G, Oyen WJG. Radioimmunotherapy for delivery of cytotoxic radioisotopes: current status and challenges. *Expert Opin Drug Deliv*. 2018;15(2):185-196. doi:10.1080/17425247.2018.1378180
28. Lin M, Paolillo V, Le DB, et al. Monoclonal antibody based radiopharmaceuticals for imaging and therapy. *Curr Probl Cancer*. 2021;45(5):100796. doi:10.1016/j.currproblcancer.2021.100796
29. Martiniova L, Zielinski RJ, Lin M, DePalatis L, Ravizzini GC. The role of radiolabeled monoclonal antibodies in cancer imaging and ADC treatment. *Cancer J*. 2022;28(6):446-453. doi:10.1097/PPO.0000000000000625
30. Parakh S, Lee ST, Gan HK, Scott AM. Radiolabeled antibodies for cancer imaging and therapy. *Cancers (Basel)*. 2022;14(6):1454. doi:10.3390/cancers14061454
31. Staudt M, Herth MM. Clearing and masking agents in pretargeting strategies. *Pharmaceuticals*. 2023;16(4):497. doi:10.3390/ph16040497
32. Li Z, Cai H, Hassink M, et al. Tetrazine–trans-cyclooctene ligation for the rapid construction of 18F labeled probes. *Chem Commun*. 2010;46(42):8043-8045. doi:10.1039/c0cc03078c
33. van de Waterbeemd H, Camenisch G, Folkers G, Chretien JR, Raevsky OA. Estimation of blood–brain barrier crossing of drugs using molecular size and shape, and H-bonding descriptors. *J Drug Target*. 1998;6(2):151-165. doi:10.3109/10611869808997889
34. Honer M, Gobbi L, Martarello L, Comley RA. Radioligand development for molecular imaging of the central nervous system with positron emission tomography. *Drug Discov Today*. 2014;19(12):1936-1944. doi:10.1016/j.drudis.2014.08.012
35. Billaud EMF, Shahbazali E, Ahamed M, et al. Micro-flow photosynthesis of new dienophiles for inverse-electron-demand Diels–Alder reactions. Potential applications for pretargeted in vivo PET imaging. *Chem Sci*. 2017;8(2):1251-1258. doi:10.1039/C6SC02933G
36. Billaud EMF, Belderbos S, Cleeren F, et al. Pretargeted PET imaging using a bioorthogonal 18 F-labeled trans-cyclooctene in an ovarian carcinoma model. *Bioconjug Chem*. 2017;28(12):2915-2920. doi:10.1021/acs.bioconjchem.7b00635
37. Ruivo E, Elvas F, Adhikari K, et al. Preclinical evaluation of a novel 18 F-labeled dTCO-amide derivative for bioorthogonal pretargeted positron emission tomography imaging. *ACS Omega*. 2020;5(9):4449-4456. doi:10.1021/acsomega.9b03584
38. Wang M, Svatunek D, Rohlfing K, et al. Conformationally strained trans-cyclooctene (sTCO) enables the rapid construction of 18 F-PET probes via tetrazine ligation. *Theranostics*. 2016;6(6):887-895. doi:10.7150/thno.14742
39. Wang M, Vannam R, Lambert WD, et al. Hydrophilic 18 F-labeled trans -5-oxocene (oxoTCO) for efficient construction of PET agents with improved tumor-to-background ratios in neurotensin receptor (NTR) imaging. *Chem Commun*. 2019;55(17):2485-2488. doi:10.1039/C8CC09747J
40. Selvaraj R, Liu S, Hassink M, et al. Tetrazine-trans-cyclooctene ligation for the rapid construction of integrin αvβ3 targeted PET tracer based on a cyclic RGD peptide. *Bioorg Med Chem Lett*. 2011;21(17):5011-5014. doi:10.1016/j.bmcl.2011.04.116
41. Selvaraj R, Giglio B, Liu S, et al. Improved metabolic stability for 18 F PET probes rapidly constructed via tetrazine trans-cyclooctene ligation. *Bioconjug Chem*. 2015;26(3):435-442. doi:10.1021/acs.bioconjchem.5b00089
42. Feng H, Zhang H, Wang M, et al. Improving tumor-to-background contrast through hydrophilic tetrazines: the construction of 18 F-labeled PET agents targeting nonsmall cell lung carcinoma. *Chem – A Eur J*. 2020;26(21):4690-4694. doi:10.1002/chem.202000028
43. Ruivo E, Adhikari K, Elvas F, et al. Improved stability of a novel fluorine-18 labeled TCO analogue for pretargeted PET imaging. *Nucl Med Biol*. 2019;76–77:36-42. doi:10.1016/j.nucmedbio.2019.11.001
44. Maggi A, Ruivo E, Fissers J, et al. Development of a novel antibody–tetrazine conjugate for bioorthogonal pretargeting. *Org Biomol Chem*. 2016;14(31):7544-7551. doi:10.1039/C6OB01411A
45. Adhikari K, Elvas F, Stroobants S, van der Veken P, Augustyns K. Development and evaluaton of a trans-cyclooctene (TCO) probe for pretargeted PET imaging. *Nucl Med Biol*. 2022;108–109:S176. doi:10.1016/S0969-8051(22)00370-5
46. Bratteby K, Shalgunov V, Battisti UM, et al. Insights into elution of anion exchange cartridges: opening the path toward aliphatic 18 F-radiolabeling of base-sensitive tracers. *ACS Pharmacol Transl Sci*. 2021;4(5):1556-1566. doi:10.1021/acsptsci.1c00133
47. Herth MM, Andersen VL, Lehel S, Madsen J, Knudsen GM, Kristensen JL. Development of a 11C-labeled tetrazine for rapid tetrazine–trans-cyclooctene ligation. *Chem Commun*. 2013;49(36):3805-3807. doi:10.1039/c3cc41027g

48. Stéen EJL, Jørgensen JT, Petersen IN, et al. Improved radiosynthesis and preliminary in vivo evaluation of the 11C-labeled tetrazine [11C]AE-1 for pretargeted PET imaging. *Bioorg Med Chem Lett*. 2019;29(8):986-990. doi:10.1016/j.bmcl.2019.02.014
49. Fukumura T, Nakao R, Yamaguchi M, Suzuki K. Stability of 11C-labeled PET radiopharmaceuticals. *Appl Radiat Isot*. 2004;61(6):1279-1287. doi:10.1016/j.apradiso.2004.04.011
50. Scott PJH, Hockley BG, Kung HF, Manchanda R, Zhang W, Kilbourn MR. Studies into radiolytic decomposition of fluorine-18 labeled radiopharmaceuticals for positron emission tomography. *Appl Radiat Isot*. 2009;67(1):88-94. doi:10.1016/j.apradiso.2008.08.015
51. Syvänen S, Lindhe Ö, Palner M, et al. Species differences in blood–brain barrier transport of three positron emission tomography radioligands with emphasis on P-glycoprotein transport. *Drug Metab Dispos*. 2009;37(3):635-643. doi:10.1124/dmd.108.024745
52. Denk C, Svatunek D, Filip T, et al. Development of a 18 F-labeled Tetrazine with favorable pharmacokinetics for bioorthogonal PET imaging. *Angew Chem Int Ed*. 2014;53(36):9655-9659. doi:10.1002/anie.201404277
53. Denk C, Svatunek D, Mairinger S, et al. Design, synthesis, and evaluation of a low-molecular-weight 11 C-labeled Tetrazine for pretargeted PET imaging applying bioorthogonal in vivo click chemistry. *Bioconjug Chem*. 2016;27(7):1707-1712. doi:10.1021/acs.bioconjchem.6b00234
54. Schlein E, Rokka J, Battisti U, et al. Synthesis and evaluation of fluorine-18 labelled tetrazines as pre-targeting imaging agents for amyloid PET-imaging. *Nucl Med Biol*. 2022;108–109:S101-S102. doi:10.1016/S0969-8051(22)00232-3
55. Shalgunov V, Lopes van den Broek S, Vang Andersen I, et al. Pretargeted imaging beyond the blood–brain barrier. RSC. *Med Chem*. 2023;14(3):444-453. doi:10.1039/D2MD00360K
56. Gupta M, Lee HJ, Barden CJ, Weaver DF. The blood–brain barrier (BBB) score. *J Med Chem*. 2019;62(21):9824-9836. doi:10.1021/acs.jmedchem.9b01220
57. Cook BE, Archbold J, Nasr K, et al. Non-invasive imaging of antisense oligonucleotides in the brain via in vivo click chemistry. *Mol Imaging Biol*. 2022;24(6):940-949. doi:10.1007/s11307-022-01744-y
58. Patra M, Zarschler K, Pietzsch H-J, Stephan H, Gasser G. New insights into the pretargeting approach to image and treat tumours. *Chem Soc Rev*. 2016;45(23):6415-6431. doi:10.1039/C5CS00784D
59. Peplow M. Click chemistry targets antibody-drug conjugates for the clinic. *Nat Biotechnol*. 2019;37(8):835-837. doi:10.1038/d41587-019-00017-4
60. Zeglis BM, Lewis JS. Click here for better chemistry. *N Engl J Med*. 2022;387(24):2291-2293. doi:10.1056/NEJMcibr2213596
61. Korat Š, Bidesi NSR, Bonanno F, et al. Alpha-synuclein PET tracer development—an overview about current efforts. *Pharmaceuticals*. 2021;14(9):847. doi:10.3390/ph14090847
62. Liu L, Johnson PD, Prime ME, et al. [11 C]CHDI-626, a PET tracer candidate for imaging mutant huntingtin aggregates with reduced binding to AD pathological proteins. *J Med Chem*. 2021;64(16):12003-12021. doi:10.1021/acs.jmedchem.1c00667
63. Liu L, Prime ME, Lee MR, et al. Imaging mutant huntingtin aggregates: development of a potential PET ligand. *J Med Chem*. 2020;63(15):8608-8633. doi:10.1021/acs.jmedchem.0c00955
64. Miyazaki T, Nakajima W, Hatano M, et al. Visualization of AMPA receptors in living human brain with positron emission tomography. *Nat Med*. 2020;26(2):281-288. doi:10.1038/s41591-019-0723-9
65. Lopes van den Broek S, Shalgunov V, García Vázquez R, et al. Pretargeted imaging beyond the blood–brain barrier—utopia or feasible? *Pharmaceuticals*. 2022;15(10):1191. doi:10.3390/ph15101191
66. Syvänen S, Fang XT, Faresjö R, et al. Fluorine-18-labeled antibody ligands for PET imaging of amyloid-β in brain. *ACS Chem Nerosci*. 2020;11(24):4460-4468. doi:10.1021/acschemneuro.0c00652
67. Sehlin D, Syvänen S. Engineered antibodies: new possibilities for brain PET? *Eur J Nucl Med Mol Imaging*. 2019;46(13):2848-2858. doi:10.1007/s00259-019-04426-0
68. Pardridge WM. Blood–brain barrier drug delivery of IgG fusion proteins with a transferrin receptor monoclonal antibody. *Expert Opin Drug Deliv*. 2015;12(2):207-222. doi:10.1517/17425247.2014.952627

How to cite this article: Zientek SH, Thompson S, Sephton SM, Aigbirhio FI. The inverse electron demand Diels–Alder cycloaddition with carbon-11 and fluorine-18: A gateway to pretargeted imaging across the blood–brain barrier. *J Label Compd Radiopharm*. 2023;1-20. doi:10.1002/jlcr.4029